ROYAL SOCIETY OF CHEMISTRY

REVIEW

Check for updates

An overview of lead-free piezoelectric materials and devices

Huige Wei,[*a] Hui Wang,[a] Yijie Xia,[a] Dapeng Cui,[*b] Yapeng Shi,[a] Mengyao Dong,[cd] Chuntai Liu,[*c] Tao Ding,[*e] Jiaoxia Zhang,[df] Yong Ma,[dg] Ning Wang,[h] Zicheng Wang,[di] Ye Sun,[j] Renbo Wei [ID][*i] and Zhanhu Guo [ID][*d]

Piezoelectric materials and devices have drawn extensive attention for energy harvesting due to their excellent electromechanical conversion properties. With increasing concerns about environmental problems in traditional lead-based piezoelectric materials, it is imperative to develop lead-free piezoelectric alternatives. This paper is intended to give a brief review on the most recent advances in both inorganic (with an emphasis on piezoelectric ceramics and ZnO nanostructures) and organic (*i.e.* polyvinylidene difluoride (PVDF) and its copolymers and their composites, and biopolymers) lead-free piezoelectric materials. State-of-the-art piezoelectric devices, namely, nanogenerators, sensors, and transducers, are also introduced with detailed examples. Finally, the challenges and perspectives of lead-free piezoelectric materials and devices are given.

1. Introduction

Piezoelectric materials, which are capable of harvesting both large and small scale energies from the environment, have attracted significant research interest in view of the energy crisis arising from the depletion of conventional fossil fuels.[1–4] The working principle of piezoelectric materials is that a potential difference is created in piezoelectric materials when a compressive or tensile force is applied, which is called a positive piezoelectric effect (Fig. 1a and b). If an electric field is applied to the piezoelectric material, a mechanical stress is produced, which is called an inverse piezoelectric effect (Fig. 1c and d).

There are several key parameters to evaluate the performance of piezoelectric materials. The first one is the piezoelectric coefficient indicating the coupling relationship

[a] College of Chemical Engineering and Materials Science, Tianjin University of Science and Technology, Tianjin 300457, China. E-mail: huigewei@tust.edu.cn

[b] College of Packing and Printing Engineering, Tianjin University of Science and Technology, Tianjin 300222, China. E-mail: dapeng@tust.edu.cn

[c] National Engineering Research Center for Advanced Polymer Processing Technology, Zhengzhou University, Zhengzhou 450002, China. E-mail: ctliu@zzu.edu.cn

[d] Integrated Composites Laboratory (ICL), Department of Chemical & Biomolecular Engineering, University of Tennessee, Knoxville, TN 37996, USA. E-mail: zguo10@utk.edu

[e] College of Chemistry and Chemical Engineering, Henan University, Kaifeng 475004, China

[f] School of Material Science and Engineering, Jiangsu University of Science and Technology, Zhenjiang, Jiangsu 212003, China

[g] College of Materials Science and Engineering, Shandong University of Science and Technology, Qingdao 266590, China

[h] State Key Laboratory of Marine Resource Utilization in South China Sea, Hainan University, Haikou 570228, China

[i] Research Branch of Advanced Functional Materials, School of Materials and Energy, University of Electronic Science and Technology of China, Chengdu 611731, China. E-mail: weirb10@uestc.edu.cn
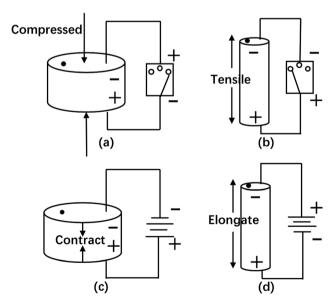
[j] Tianjin Morgan-Kundom Hi-Tech Development Co., Ltd., Tianjin 300457, China

Fig. 1 Schematic of the positive and inverse piezoelectric effects. (a) and (b) show the positive piezoelectric effect applied by a compressive and tensile force, respectively. (c) and (d) show an inverse piezoelectric effect which causes the piezoelectric material to contract and elongate, respectively.

between mechanical properties and dielectric properties of piezoelectric bodies. The piezoelectric coefficient is usually denoted as d_{xy}, where x and y represent the direction of the electric field and the direction of the stress or strain, respectively. For example, the longitudinal piezoelectric coefficient (d_{33}),[5] transverse piezoelectric coefficient (d_{31}),[6] and tangential piezoelectric coefficient (d_{15})[7] are usually reported in the literature. A second parameter is the electromechanical coupling coefficient (k) standing for the degree of energy transformation. The planar electromechanical coupling factor (k_p),[8] transverse electromechanical coupling factor (k_{31}),[9] longitudinal electromechanical coupling factor (k_{33}),[10] or thickness electromechanical coupling coefficients (k_t)[11] are provided by researchers. Some other parameters include the dielectric constant (ε_r), Curie temperature (T_c), depolarization temperature (T_d), remanent polarization (P_r), spontaneous polarization $(P_s$, the intensity of polarization already possessed by each electric domain), resistance (R) and dielectric dissipation factor $(\tan \delta)$.[12] High performance piezoelectric materials are usually characterized with high d_{33}, k, ε_r, T_c, T_d, and P_r, and low R and $\tan \delta$.

Lead zirconate titanate (PZT) was the first studied lead-based piezoelectric material,[13] followed by others such as lead metaniobate,[14] lead titanate,[15] lead barium lithium niobate,[16] and modified lead titanate.[17] PZT has become the mainstream of lead-based piezoelectric materials due to its desirable elastic, dielectric, piezoelectric, pyroelectric, ferroelectric, and optical properties.[18–22] Unfortunately, the content of lead in these lead-based piezoelectric materials has an adverse effect on human beings and ecosystems, and therefore, lead-free piezoelectric materials have drawn increasing attention in recent years. Till now, both inorganic (such as piezoelectric ceramics[23–25] and ZnO nanostructures[26–28]) and organic (for example, piezoelectric polymers or some polymer nanocomposites[29,30]) lead-free piezoelectric materials have been explored. These lead-free materials exhibited comparable or even superior piezoelectric properties compared with PZT. Moreover, they are environmental friendly and biocompatible, and are expected to completely replace their lead-based counterparts in the near future.

With advances in technologies for preparing a myriad of materials with tunable piezoelectric properties, novel piezoelectric

Huige Wei

Dr Huige Wei, currently an Associate Professor in the College of Chemical Engineering and Materials Science at Tianjin University of Science and Technology, Tianjin, China, obtained her PhD degree from Dan F. Smith Department of Chemical Engineering at Lamar University, USA (2015). Her current research focuses on multi-functional composites for energy conversion and storage applications.

Hui Wang

Hui Wang, currently a master's student in the Department of College of Chemical Engineering and Materials Science at Tianjin University of Science and Technology (TUST), Tianjin, China, obtained his bachelor's degree from TUST in 2017. His current research focuses on multi-functional polymer composites for energy conversion and storage applications.

Dapeng Cui

Dr Dapeng Cui, currently an Assistant Professor in the College of Packing and Printing Engineering at Tianjin University of Science and Technology, Tianjin, China, obtained his PhD degree from Department of Chemistry and State Key Laboratory of Applied Organic Chemistry, Lanzhou University, China. He received three-year (2011–2014) postdoctoral training in Laboratory of New Materials, Institute of Chemistry, Chinese Academy of Sciences, Beijing, China. His current research focuses on flexible and printed electronics and devices, bio-inspired hirachical nanostructures.

Chuntai Liu

Dr Liu Chuntai is the professor of materials processing engineering, deputy director of national engineering research center for advanced polymer processing technology, Zhengzhou University. He received a BS degree in Mechanics from Peking University, a MS degree in Engineering Mechanics from Xi'an Jiaotong University, and a PhD degree in Material Science and Engineering from Zhengzhou University. He was a visiting scholar in Ohio State Univ. from 2006 to 2007. His recent research fields include multi-scale modeling and calculating of polymer processing; physical problems of polymer processing; lightweight and functional nanocomposites, etc.

This journal is © The Royal Society of Chemistry 2018

J. Mater. Chem. C, 2018, **6**, 12446–12467 | **12447**

devices have been proposed. These devices find promising applications in the fields of bioengineering, military, opto-electronic information, and energy.[31–34] For instance, pressure sensors using piezoelectric PVDF composites were used to detect the situation outside the fuselage.[35] Piezoelectric nano-generators based on ZnO nanowires were able to monitor cell health through the conversion of mechanical energy produced by body motion and muscle contraction into electrical energy.[36]

Some review papers summarized the progress of some lead-free piezoelectric ceramics,[37–39] but other important lead-free piezoelectric materials, for example, organic piezoelectric poly-mers, were not included; and piezoelectric devices have rarely been introduced. In this content, this paper is intended to give a comprehensive review on most advances of lead-free piezo-electric materials and innovative devices. First, a review on the most recent advances in both inorganic (with an emphasis on piezoelectric ceramics and ZnO nanostructures) and organic (*i.e.* PVDF and its copolymers and their composites, and biopolymers) lead-free piezoelectric materials is presented. Then, state-of-the-art piezoelectric devices, namely, nano-generators, sensors, and transducers, are introduced. Finally, the challenges and perspectives of lead-free piezoelectric materials and devices are given.

2. Research progress in lead-free piezoelectric materials

Generally, lead-free piezoelectric materials are classified into two categories: inorganic and organic. This review paper focuses on typical inorganic ceramics (*i.e.* barium titanate (BT) based-, sodium potassium niobate (KNN) based-, and sodium bismuth titanate (BNT) based-ceramic systems and bismuth layer-structured ferroelectrics (BLSFs)) and ZnO nanostructures. In the case of organic lead-free piezoelectric

materials, PVDF and its copolymers and their composites, and some biopolymers are introduced.[40–46]

2.1 Inorganic lead-free piezoelectric ceramics

2.1.1 BT-Based ceramic system. The BT-based ceramic system with an ABO_3 perovskite structure (A is calcium, stron-tium, barium, *etc.*, and B is niobium, tantalum, titanium, *etc.*) is the first reported lead-free piezoelectric ceramic.[47] At room temperature, the BT-based ceramic system has advantages of stable electrical properties, good electromechanical coupling and low dielectric loss, but is limited by low T_c and d_{33}.[48] Improved piezoelectric properties have been achieved by designing novel structures or optimizing the preparation procedure.[49–51] For example, using a sol–gel method, Praveen *et al.*[52] found that the phase composition of barium zirconate titanate–barium calcium titanate (BZT–BCT) was better controlled, giving rise to reduced processing temperatures and finer particle size. The product had a high P_r of 12.2 μC cm^{-2}, a high d_{33} of 637 pC N^{-1}, and a large k_p of 0.596. Roscow *et al.*[53] reported sandwich-structured piezoelectric BT where a porous layer of BT was sandwiched between two dense outer layers of BT. The remark-able difference in the effective permittivity between the porous and dense layer caused high field concentrations in the former, leading to varied piezoelectric properties as a function of the porosity of the interlayer and the relative thickness (the ratio of the interlayer thickness to that of the planar structure). An optimum d_{33} (124.5 pC N^{-1}) was achieved at a 60 vol% porosity of the interlayer and a relative thickness of 0.52.

Doping modification has become an important strategy to accomplish high performance piezoelectric ceramics by introducing appropriate donors to acceptors in the ceramic. The improved piezoelectric properties are attributed to the newly formed morphotropic phase boundary (MPB) in the doped ceramics. The electric domains of the MPB have many polarization

Ye Sun, currently working at Research and Development division of Tianjin Morgan-Kundom Hi-Tech Development Co., Ltd. Tianjin, obtained his master's degree from Tianjin University of Science and Technology. His work mainly focuses on silicon dioxide for coating and thermal insulation applications.

Ye Sun

Dr Zhanhu Guo, currently an Associate Professor in Depart-ment of Chemical and Biomole-cular Engineering, University of Tennessee, Knoxville, USA, obtained a PhD degree in Chemical Engineering from Louisiana State University (2005) and received three-year (2005–2008) postdoctoral training in Mechanical and Aero-space Engineering Department at University of California Los Angeles. Dr Guo directs the Integrated Com-posites Laboratory and chairs the

Zhanhu Guo

Composite Division of American Institute of Chemical Engineers (AIChE, 2010–2011). His current research focuses on fundamental science behind multifunctional light-weight nanocomposites especially with polymer and carbon as the hosting matrix for electronic devices and environmental remediation applications.

12448 | *J. Mater. Chem. C*, 2018, **6**, 12446–12467

This journal is © The Royal Society of Chemistry 2018

directions, making it easier for them to be oriented under the action of an electric field force.[54–57] Zhu et al.[58] observed the MPB between the pseudocubic (PC) and the rhombohedral (R) phase in $BaTiO_3$–$BiFeO_3$ (BF–BT) doped by $Bi(Mg_{0.5}Ti_{0.5})O_3$ (BMT). The optimum phase composition was achieved when the ratio of BF, BT and BMT was 1 : 1 : 0.04. Correspondingly, d_{33} and T_c reached 154 pC N^{-1} and 482 °C, respectively.

In recent years, in order to overcome the brittleness and the incompatibility with irregular mechanical deformations, incorporating piezoelectric ceramics into soft and flexible polymer matrixes has become a popular approach.[59–61] For example, BC is well known for its good mechanical strength, chemical stability and high crystallinity as a biopolymer.[62] Because of the textured nanofibrillated structure of BC, it is often used as a reinforcement or matrix to fabricate functional composites.[63,64] Zhang et al.[65] fabricated BT/BC piezoelectric composites using a facile vacuum filtration method (Fig. 2a–g). The piezoelectric BT nanoparticles were uniformly distributed in the matrix of percolated networks of BC nanofibers. The nanogenerator based on this unique structure of BT/BC gave a maximum power density (P) of 0.64 μW cm^{-2}, which was ten times higher than that of BT/polydimethylsiloxane.

2.1.2 KNN-Based ceramic system. The KNN-based ceramic system has been considered as one of the most promising lead-free piezoelectric materials because of its decent overall performance such as high T_c (420 °C), high P_r (33 μC cm^{-2}) and large k_p ($\sim$0.454).[66,67] The KNN-based ceramic system is usually prepared by a solid-state method, which is known for its simplicity.[68] However, it requires a very high temperature (1000–1500 °C); meanwhile, the purity and performance of the product is not satisfying. Therefore, other methods such as normal sintering,[69] a wet chemical method,[70] and a seed-free solid-state crystal growth method,[71] have been developed to overcome these shortcomings. Using the normal sintering approach, Zhang et al.[72] prepared $0.96(K_{0.5}Na_{0.5})_{0.95}Li_{0.05}Nb_{1-x}Sb_xO_3$–$0.04BaZrO_3$, and the products had a higher purity ($>$99.5%) than that obtained by the solid-state method (usually around 90%).

Recently, in order to avoid problems of deliquescence and volatility of alkaline oxides associated with KNN-based ceramics prepared by normal sintering,[73,74] cutting-edge technologies, e.g. spark plasma sintering (SPS), sealed sintering, and microwave sintering have been developed.[75–79] Moreover, these approaches have other advantages. For instance, SPS features a fast sintering speed, low sintering temperature, high reproducibility, and short dwell time.[80] Sealed sintering yields products with high purity,[81] while microwave sintering significantly reduces the processing time.[82] Feizpour et al.[82] compared the $(K_{0.5}Na_{0.5})NbO_3$ ceramics obtained via the microwave sintering and the traditional sintering methods. Negligible difference in these piezoelectric properties was observed but the volatility of the product via microwave sintering was improved; meanwhile, the sintering time of microwave sintering was only 3% of the traditional sintering time.

To further improve the piezoelectric properties of the KNN-based ceramic system, a post processing method of domain engineering was used, i.e. to manipulate the domain structure by applying an electric field to the obtained ceramics.[83] The increased density of domain walls lowered the potential barrier of polarization switching, and thus contributed to enhanced piezoelectric properties.[84] For instance, in order to enhance the piezoelectric properties of 0.5 wt% Mn–KNN, Lin et al.[85] used the field-cooling, that is, to apply an electric field and then cool the sample at a certain rate, domain engineering method. Samples with different domain sizes and piezoelectric properties (Fig. 3a–d) could be obtained by adjusting the electric field strength, temperature and cooling rate. d_{33} and T_c of the product reached up to 350 pC N^{-1} and 416 °C, respectively. Nevertheless, the domain engineering technique is not suitable for ceramics of small single crystal size.[86] Therefore, it is of
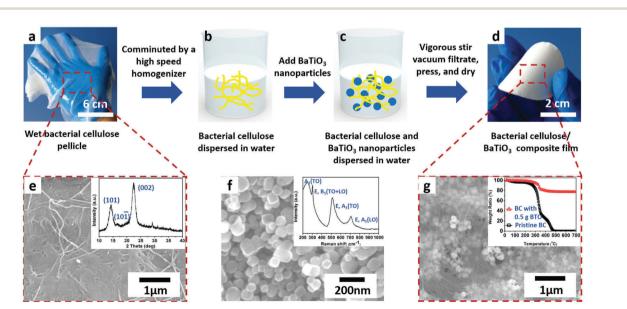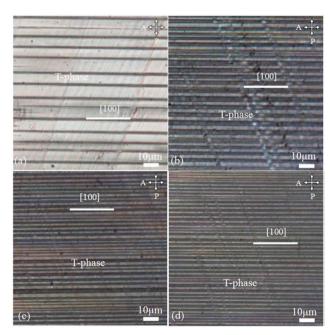

Fig. 2 (a–d) The preparation process of the BT/BC composite film. (e) The SEM image and XRD pattern (the inset) of the original BC film. (f) The SEM image and Raman spectrogram of BT nanoparticles. (g) The SEM image and TGA (the inset) of the composite film.

This journal is © The Royal Society of Chemistry 2018

J. Mater. Chem. C, 2018, 6, 12446–12467 | 12449

Fig. 3 The [001]-oriented Mn-KNN crystal domain was observed at 205 °C under different electric fields along the [001] direction (a) $E = 0$, (b) $E = 6$, (c) $E = 12$, and (d) $E = 18$ kV cm^{-1}. Reprinted from ref. 85 with permission from AIP Publishing.

particularly importance to increase the size of the single crystal. Tantalum is often used to facilitate the growth of single crystals of KNN-based ceramics.[87] Zheng et al.[86] prepared a large-sized, high-quality tantalum-modified single crystal (K, Na)(Nb, Ta)O$_3$ (KNNT) by top-seeded solution growth (TSSG). The dimensions of this KNNT single crystal reached 12 × 11 × 11 mm which were greater than those of KNN (the diameter was 4 mm) not modified by tantalum. k_{33} and k_t of the (K, Na)(Nb, Ta)O$_3$ (KNNT) single crystal reached 0.827 and 0.646, respectively, even higher than those of PZT ($k_{33} = 0.68$, $k_t = 0.507$).

2.1.3   BNT-Based ceramic system. As a lead-free piezoelectric material, the BNT-based ceramic system is well known for its large P_r (38 μC cm^{-2}) and high T_c (320 °C). Therefore, the BNT-based piezoelectric system has received widespread attention in the field of piezoelectricity.[88] Particularly, the BT-modified $(1-x)$(Na$_{0.5}$Bi$_{0.5}$)TiO$_3$–xBaTiO$_3$ system (NBBT) has been considered as the most promising one.[89] Unfortunately, the NBBT monocrystal is still limited for many applications arising from its large leakage current, serious dielectric loss and low T_d. In recent years, NBBT with larger single crystal size

displayed better piezoelectric properties due to fewer oxygen vacancies which led to reduced leakage current.[86] Zheng et al.[90] obtained a large-sized and high-quality 0.95(Na$_{0.5}$Bi$_{0.5}$)TiO$_3$–0.05BaTiO$_3$ (NBBT95/5) monocrystal in the rhombohedral phase by TSSG. The [001]$_c$ poled NBBT95/5 multidomain single crystal showed a significant piezoelectric effect (d_{33} = 360 pC N^{-1}, d_{15} = 162 pC N^{-1}, and d_{31} = −113 pC N^{-1}), high k (k_{33} = 0.720, and k_t = 0.540), low tan δ (1.1%) and high T_d (135 °C), which proved to be a promising candidate to replace the PZT ceramic in many fields. Xue et al.[91] prepared a Fe-doped NBBT single crystal to enhance the piezoelectric properties. d_{33} of the 0.2 at% Fe-doped monocrystal material increased from 420 to 590 pC N^{-1}. Doping with Fe-ions gave rise to evolution from macrodomains to nanodomains, which greatly improved the piezoelectric properties of NBBT.

In addition to the NBBT, there are many other types of BNT-based ceramics which have attracted increasing attention. For instance, Bai et al.[92] synthesized a [00l]-textured 0.83Na$_{0.5}$Bi$_{0.5}$TiO$_3$–0.17Bi$_{0.5}$K$_{0.5}$TiO$_3$ (BNT–BKT) ceramic by the template grain growth (TGG) method which used BaTiO$_3$, SrTiO$_3$ and NaNbO$_3$ anisotropic particles as template particles. The resulting [001]-textured BNT–BKT ceramic had a large equivalent piezoelectric coefficient (S_{max}/E_{max} = −710 pm V^{-1}) at room temperature at a low driving field of 45 kV cm^{-1}, and the thermal stability of the ceramic at high temperature was also enhanced. Li et al.[93] prepared a novel ceramic of 0.94(Bi$_{0.5}$Na$_{0.5}$)TiO$_3$–0.06BaTiO$_3$–xBi$_4$Ti$_3$O$_{12}$ (BNT–BT–xBiT). Bi$_4$Ti$_3$O$_{12}$ (BiT) was selected as the third end member given its both high P_s (>30 μC cm^{-2}) and T_c (~675 °C). Meanwhile, sheet-shaped BiT facilitated the grain growth, as confirmed by the SEM images of the samples with different BiT contents (Fig. 4a–d). After the testing, a solid solution was formed by the diffusion of BiT into the lattice of BNT–BT. The sample of BNT–BT–6 wt% BiT showed the largest strain response (d_{33} = −465 pm V^{-1}). This lead-free system provided an effective way to increase the strain response of piezoelectric ceramics.

2.1.4   Bismuth layer-structured ferroelectrics (BLSFs). BLSFs are piezoelectric ceramics with a crystalline structure composed of (Bi$_2$O$_2$)$^{2+}$ layers and (A$_{m-1}$B$_m$O$_{3m+1}$)$^{2-}$ layers arranged alternately along the c axis, where A could be K$^+$, Na$^+$, Ca^{2+}, Sr^{2+}, Pb^{2+}, Ba^{2+}, Ln^{3+}, Bi^{3+}, Ce^{4+}, etc., and B could be Fe^{3+}, Cr^{3+}, Ti^{4+}, Nb^{5+}, Ta^{5+}, W^{6+}, Mo^{6+}, etc.[94] The BLSFs were discovered by Aurivillus in 1949, and have drawn extensive attention since then.[95] BLSFs have merits of high T_c, low tan δ, low ε_r and decent aging resistance.[96] BaBi$_4$Ti$_4$O$_{15}$ (BBT) belongs to one type of BLSFs.
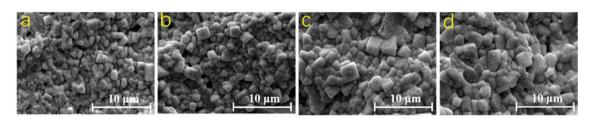

Fig. 4 The SEM images of BNT–BT–xBiT samples with various contents of Bi$_4$Ti$_3$O$_{12}$. (a) 0, (b) 3, (c) 5, and (d) 6 wt%. Reproduced from ref. 93 with permission from Elsevier Ltd.

BBT first reported by Subbarao et al.[97] had a T_c of about 395 °C but the piezoelectric activity was low (d_{33} = 12 pC N^{-1}). The piezoelectric properties of BBT ceramics were found to be notably improved by modification with cerium (Ce).[98] Diao et al.[99] prepared a series of Ce-modified BBT ceramics with different contents of Ce through a high temperature solid-state method. The 0.50 wt% Ce-modified BBT ceramics had the best performance, and T_m and d_{33} were 407 °C and 24.2 pC N^{-1}, respectively.

Another typical member of the BLSF family is CaBi$_4$Ti$_4$O$_{15}$ (CBT).[100] CBT has a high T_c (790 °C) but a poor piezoelectric property (d_{33} = 8 pC N^{-1}). Shen et al.[101] fabricated B-site Nb-doped and Nb/Mn co-doped CBT ceramics (CBTN–Mn) by the conventional solid-state method. d_{33} and T_c of CBTN–Mn reached 23 pC N^{-1} and 790 °C respectively. At the same time, tan δ was reduced from 0.8 to 0.2% and the resistivity was increased from 5.7 × 10^5 to 4.2 × 10^6 Ω at 500 °C. Therefore, CBTN–Mn ceramics are perceived to be of promising potential in the field of high temperature induction and braking.

Yet, there are some deficiencies of BLSFs. First, the coercive electric field of BLSFs is relatively high so that they are difficult to polarize. Second, the steering of spontaneous polarization is subjected to two-dimensional confinement because of the crystal structure characteristics, which makes the piezoelectric activity of BLSFs low.[102] At present, efforts to improve the piezoelectric properties of BLSFs are generally classified into two aspects: one is to optimize the preparation process and the other is by ion doping. For example, the conventional solid-state method is usually employed to prepare BBT, and the sintering temperature was found to have great influence on the piezo-electric properties.[103] Khokhar et al.[104] found BBT ceramics sintered at 1050 °C featured a denser microstructure compared with their counterparts sintered at other temperatures, i.e. 950, 1000, and 1100 °C (Fig. 5a–d), and a higher resistivity (4.6 × 10^{12} Ω cm), lower tan δ (0.05), larger P_r (3.63 μC cm^{-2})

and larger d_{33} (24 pC N^{-1}) were also achieved. Doping was capable of forming a MPB leading to better piezoelectric performance.[105] Xiao et al.[106] used a conventional solid-state method to synthesize (Li,Ho)-doped CBT multifunctional ceramics, namely, Ca$_{1-x}$(Li,Ho)$_{x/2}$Bi$_4$Ti$_4$O$_{15}$. The properties of the ceramics varied with changing the factor of x. The optimum comprehensive performance was achieved when x = 0.1 (R = 4.51 × 10^{11} Ω cm, d_{33} = 10.2 pC N^{-1}, T_c = 814 °C, and P_r = 9.03 μC cm^{-2}). By comparing the aforementioned two ways to improve piezoelectric performance, it is found that optimi-zation of the preparation process has a greater influence on d_{33}, while the doping method affects significantly T_c. The former is simpler to operate, but the reaction conditions are more demanding, while the latter is the opposite.

2.1.5 ZnO nanostructures. ZnO is also an important lead-free piezoelectric material with advantages of pollution-free and multiplicity of processing, which are unmatched by PZT.[107] ZnO nanostructures have received lots of attention due to their distinguished properties in piezoelectrics, electronics and photonics.[108–112] These properties are attributed to surface and quantum confinement effects.[113] Hsu et al.[114] reported a facile method to prepare ZnO nanostructures. They successfully synthesized ZnO nanostructures on silicon wafers by a chemical solution deposition (CSD) with two-step thermal-oxidation approach, which could be finished within one hour. In the CSD process, three-shaped ZnO nanostructures (dandelion-like nanostructures, columnar nanostructures and nanowires) could be obtained by adjusting the mixing ratio of Zn particles to the volume of oxalic acid solution. Fig. 6 shows the SEM images of dandelion-like ZnO nanostructures grown in 10 mL oxalic acid solution at different oxidizing temperatures. Both the average diameter and length of the nanostructures increased with increasing the oxidizing temperature.

For the past few years, patterned low-dimensional nano-materials have aroused wide interest due to their uniform

Fig. 5 Microstructure of BBT sintered at varying temperatures. (a) 950, (b) 1000, (c) 1050, and (d) 1100 °C. Reproduced from ref. 104 with permission from Elsevier Ltd.
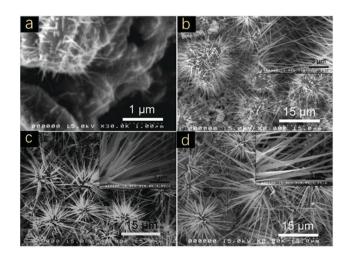

Fig. 6 SEM images of synthesized ZnO nanostructures using 10 mL oxalic acid solution at oxidizing temperatures of (a) 350, (b) 500, (c) 600, and (d) 700 °C for 20 min. Reproduced from ref. 114 with permission from Elsevier Ltd.

This journal is © The Royal Society of Chemistry 2018

J. Mater. Chem. C, 2018, 6, 12446–12467 | 12451

(1) One-step residue-free patterning in polymer film

Si master

0.5 μm

2.1 μm   <10 nm   20~70 nm

polymer film 40~60 nm

ZnO-coated Si or cs-ZnO substrate

(2) Post annealing

50~300 nm

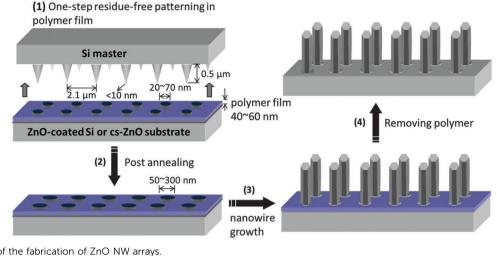**(3)** nanowire growth

(4) Removing polymer

Fig. 7 Schematic of the fabrication of ZnO NW arrays.

morphology and structure, controllable size, permutation cycle, and orientation.[115,116] Zhao et al.[117] reported a non-conventional nanopatterning technique combined with hydro-thermal synthesis to prepare ZnO NWs with high uniformity and vertical alignment. As is shown in Fig. 7, a PS film on a single crystal ZnO substrate was lightly touched with a fluori-nated Si stamp containing conical-shaped sharp tip arrays, and hollow circular patterns were formed in the contact area. The opening diameter was adjusted by thermal annealing. The nanowires were generated by the hydrothermal synthesis method. Finally, the polymer film was removed to obtain the product. This method had good economic benefits since subsequent operations such as etching, which was necessary for other lithography techniques, were avoided. The surface pattern sizes were regulated by controlling the patterning parameters or applying post-thermal annealing. The nanowires prepared by this method have unique semiconductor-piezoelectric properties, which laid a good founda-tion for the future application of nanomaterials. In addition, Wang et al.[118] employed a mechanoelectrospinning-assisted direct-writing process and hydrothermal growth process to fabri-cate patterned ZnO nanorod arrays. The structure of ZnO nanorod arrays was controlled by altering the hydrothermal reaction time and the printing conditions. Moreover, this method had merits of low cost, mild temperature, and eco-friendliness, and a template was not needed as well.

Meanwhile, ZnO also serves as an important filler to improve the piezoelectric properties of polymers, for example, polyvinylidene fluoride (PVDF). The incorporation of ZnO increased the defects of PVDF chains, leading to enhanced piezoelectric responses.[119] Bhunia et al.[120] deposited a nano-ZnO/PVDF free-standing flexible composite film via the sol–gel technique. After polarization, the output voltage of the compo-site film increased by ten times whereas that of the PVDF film doubled. However, the maximum power and the electric current were reduced due to the higher resistance arising from the introduction of nano-ZnO to the PVDF polymer.

2.1.6 Other inorganic lead-free piezoelectric materials. Other lead-free piezoelectric materials include ceramics with

a formula of $A_xB_2O_6$ (A is calcium, strontium, barium, etc., and B is niobium, tantalum, titanium, etc.). Ceramics based on $Sr_{2-x}Ca_x$–$NaNb_5O_{15}$ (SCNN) were also reported to have great potential in the field of mechanical and electrical applications.[121] Recently, $ZnSnO_3$ emerged to be a promising lead-free perovskite piezoelectric material with high remnant polarization and excellent energy-harvesting capacity.[122] P_r of $ZnSnO_3$ reaches as high as 59 μC cm^{-2}. In addition, $ZnSnO_3$ does not require electric field polarization since it exhibits self-poling behavior under mechanical strain.[123]

Table 1 summaries the main parameters of the inorganic lead-free piezoelectric materials involved in this paper. It is encouraging that the performance of lead-free piezoelectric materials catches up with lead-based piezoelectric materials, so it is expected that lead-free piezoelectric materials will replace lead-based piezoelectric materials in the near future.

2.2 Organic lead-free piezoelectric materials

Organic lead-free piezoelectric materials, sometimes referred to as piezoelectric polymers,[124] mainly include PVDF and other organic piezoelectric materials such as epoxy, nylon, and silicone.[125–127] Particularly, PVDF and its copolymers and their composites have received enormous research interest in recent years due to their advantages of low density, good flexibility, low impedance and large piezoelectric constant.[128–130] With these merits, they have now been widely used in manufacturing ultrasonic transducers,[131] electroacoustic transducers,[132] ceramic filters,[133] infrared detectors,[134] etc.

2.2.1 PVDF-based piezoelectric materials

2.2.1.1 PVDF and its copolymers. PVDF is widely used as a piezoelectric material for its larger d_{33} (20–28 pC N^{-1}) com-pared with that of other polymers.[135] Besides, PVDF has strong polarity, excellent piezoelectric and mechanical properties, and stable chemical properties.[136] PVDF has three phases of α, β, and γ, of which only the β phase exhibits piezoelectric properties.[137–139] PVDF is traditionally prepared by emulsion and suspension polymerization methods.[140–143] However, the PVDF produced by these approaches has a low content of

12452 | J. Mater. Chem. C, 2018, 6, 12446–12467

This journal is © The Royal Society of Chemistry 2018

Table 1 A literature survey of the main parameters of inorganic lead-free piezoelectric materials

Category	Composition	Preparation method	d_{33} (pC N^{-1})	T_c (°C)	k	P_r (μC cm^{-2})	$\tan\delta$	T_d (°C)	Ref.
BT-Based ceramic system	$x\mathrm{Ba(Zr_{0.2}Ti_{0.8})O_3}$–$(1-x)\mathrm{(Ba_{0.7}Ca_{0.3})TiO_3}$	Sol–gel method	637		0.596	12.20			52
	BF–BT–$x\mathrm{Bi(Mg_{1/2}Ti_{1/2})O_3}$	High temperature sintering	184	482	0.285	16.20	0.084		58
KNN-Based ceramic system	$0.96\mathrm{(K_{0.5}Na_{0.5})}0.95\mathrm{Li_{0.05}Nb_{1-x}Sb_xO_3}$–$0.04\mathrm{BaZrO_3}$	Normal sintering	425	197	0.500	15.80	0.032		72
	0.5 wt% Mn–$\mathrm{(K_{0.5}Na_{0.5})NbO_3}$	Field-cooling domain engineering method	350	416			3.500		85
	$\mathrm{(Na,K)(Nb,Ta)O_3}$	TSSG	200	291	0.827		0.004		86
BNT-Based ceramic system	$0.95\mathrm{(Na_{1/2}Bi_{1/2})TiO_3}$–$0.05\mathrm{BaTiO_3}$	TSSG	360		0.720	38.00	1.100	135	90
	Fe-Doped $0.95\mathrm{(Na_{1/2}Bi_{1/2})TiO_3}$–$0.05\mathrm{BaTiO_3}$	TSSG	600			40.00			91
	$0.83\mathrm{Na_{0.5}Bi_{0.5}TiO_3}$–$0.17\mathrm{Bi_{0.5}K_{0.5}TiO_3}$	Template grain growth method	161			34.00		72	92
	$0.94\mathrm{(Bi_{0.5}Na_{0.5})TiO_3}$–$0.06\mathrm{BaTiO_3}$–$x\mathrm{Bi_4Ti_3O_{12}}$ (BNT–BT–xBiT)	Conventional solid-state method	152	675			0.150		93
BLSFs	$\mathrm{BaBi_4Ti_4O_{15}}$–$x\mathrm{CeO_2}$	High temperature solid-state method	24.2	407			0.023		99
	$\mathrm{CaBi_4Ti_{3.95}Nb_{0.05}O_{15}}$ + 0.2 wt% $\mathrm{MnO_2}$	Conventional solid-state method	23	790	0.047		0.200		101
	$\mathrm{BaBi_4Ti_4O_{15}}$	High temperature sintering	24	395	0.036		0.050		104
	$\mathrm{Ca_{1-x}(Li,Ho)_{x/2}Bi_4Ti_4O_{15}}$	Conventional solid-state method	10.2	814		9.03			106

the β phase, resulting in poor piezoelectric performance. Therefore, a lot of study has been carried out to improve the piezoelectric properties of PVDF by increasing the content of the β phase. For example, some nucleating agents (*e.g.* montmorillonite, multi-walled carbon nanotubes, MoS_2, and LiCl)[144–146] were employed. Mao *et al.*[147] prepared a sponge-like mesoporous piezoelectric PVDF thin film with the aid of ZnO nanoparticles (NPs) to enhance the piezoelectric performance of PVDF. This mesoporous PVDF film was fabricated by casting a mixture of PVDF and ZnO nanoparticles (NPs) onto a flat surface, and the ZnO NPs were later etched using HCl acid solution (Fig. 8). ZnO NPs could not only adjust the mechanical properties of the PVDF film by creating pores but also helped to form a piezoelectric β phase. The polar surface of ZnO NPs interacted with CH_2 and CF_2 groups of PVDF with positive and negative charge density, respectively, thereby triggering β-phase nucleation. Some efforts were made towards optimizing the heat treatment process of PVDF when conventional polymerization methods were employed.[148–150] Tiwari *et al.*[151] found that quenching temperatures could affect the crystallinity of PVDF and the content of the β phase. A maximum content of the β phase in PVDF was achieved at a quenching temperature

of 20 °C. New methods have also been explored aiming to produce PVDF with a high content of the β phase.[152–154] Using a simple phase inversion technique, Soin *et al.*[155] obtained almost pure β-phase PVDF after the sample was quenched at a temperature of −20 °C. The piezoelectric properties of PVDF films prepared by this method were greatly improved and the absolute value of piezoelectric coefficient d_{33} reached as high as −49.6 pm V^{-1}, whereas d_{33} of common PVDF film was only around 18 pC N^{-1}.

Other problems associated with traditional preparation methods such as emulsion polymerization are the large amounts of waste water generated and lots of energy consumed to dry the polymer.[156,157] To overcome these shortcomings, Wolff *et al.*[158] proposed a new rapid expansion of supercritical solutions (RESS) to generate PVDF piezoelectric polymer particles. The polymer was first dissolved in supercritical CO_2 to form a homogeneous supercritical mixture, and then was rapidly expanded to atmospheric conditions through a heated capillary nozzle (338 K, the inner diameter was 50 mm). A spontaneous phase change and formation of polymer particles occurred during the expansion process. As is shown in Fig. 9a and b, the PVDF particle size prepared by this method was reduced by
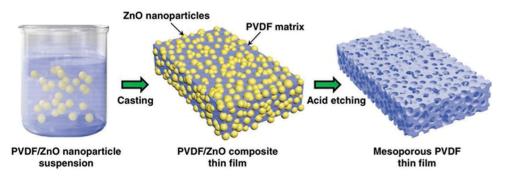

Fig. 8 Schematic of fabricating mesoporous piezoelectric PVDF thin films. Reproduced from ref. 147 with permission from John Wiley and Sons Ltd.
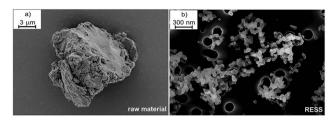
This journal is © The Royal Society of Chemistry 2018

J. Mater. Chem. C, 2018, **6**, 12446–12467 | 12453
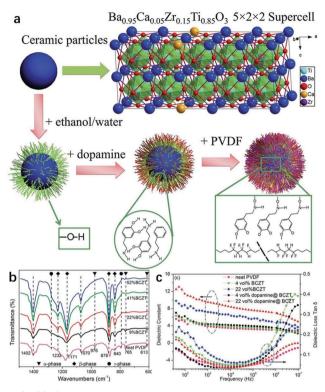
Fig. 9 SEM images of PVDF (a) prior and (b) after RESS.

about 300 times compared to that by the emulsion method. The content of the β phase in PVDF products was also greatly increased and the content of the α phase was reduced as confirmed by XRD and FTIR results, suggesting that RESS could promote the transformation of α- to β-phase PVDF.

PVDF copolymers such as poly(vinylidene fluoride-hexa-fluoropropylene), or P(VDF-HFP),[159] poly(vinylidene fluoride-trifluoroethylene), or P(VDF-TrFE),[160] and poly(vinylidene fluoride-tetrafluoroethylene), or P(VDF-TeFE)[161] have received extensive attention. Particularly, P(VDF-TrFE) has been widely studied due to its better piezoelectricity and flexibility.[162] Whiter et al.[163] prepared aligned P(VDF-TrFE) nanowires by a cost-effective template wetting method. With the aid of commercially available anodized nanoporous aluminum (AAO) film, aligned P(VDF-TrFE) nanowires with a diameter of 196 ± 18 nm in the pores and a d_{33} of 35 pC N^{-1} were obtained.

2.2.1.2 PVDF-based composites. In 1978, R.E. Newnham[164] first proposed the concept of piezoelectric ceramic/polymer composites. Up to now, polymer matrixes including PVDF,[165] polyamide,[166] epoxy,[167] and silicone polymer,[168] have been developed, among which PVDF is the most studied.

The flexibility and designability of the PVDF matrix make up for the short plates of traditional rigid piezoelectric materials (*e.g.* piezoelectric ceramics) and therefore expand their application scope. PVDF proves to be an excellent polymer matrix for fabricating advanced piezoelectric composites, for which fillers such as carbon nanotubes, graphene, BaTiO$_3$, SiO$_2$, and TiO$_2$ have been studied.[169–173] The sol–gel method, hot-press approach, solution casting method, *etc.*, have been developed to prepare PVDF-based piezoelectric composites. For instance, in the sol–gel method, the reaction is ready to proceed, the reaction temperature is low, and the product is relatively uniform. However, it is time consuming and expensive raw materials are generally required; besides, a large number of micropores are usually generated which would shrink, leading to reduced piezoelectric performance.[174,175] The obtained products of the hot-press method have advantages of high compactness, easy orientation, and low porosity. Compared with the extrusion, wet-chemical and other polymer processing methods, the shortcomings of hot press are low productivity and high cost.[176–178]

The solution casting method is also one of the most used methods to prepare PVDF-based piezoelectric composites. This method is simple, fast and low cost, but the products usually contained impurities of solvent.[179,180] Using the solution casting method, Luo et al.[181] fabricated a Ba$_{0.95}$Ca$_{0.05}$Zr$_{0.15}$Ti$_{0.85}$O$_3$/PVDF

Fig. 10 (a) Schematic diagrams of the fabrication of the dopamine@BCZT/PVDF composite. (b) FT-IR spectra and (c) dielectric constant and dielectric loss tangent dependence on frequency for dopamine@BCZT/PVDF and BCZT/PVDF composite films.

composite film with dopamine as a coupling agent (dopamine@BCZT/PVDF) with a thickness of 20–100 μm (Fig. 10a). The content of the β phase increased with the increase of BCZT content as confirmed by the infrared spectrum (Fig. 10b). The dielectric constant of the film increased with increasing BCZT content. By the introduction of the coupling agent of dopamine, the dielectric constant was further increased, and the dielectric loss angle turned completely opposite (Fig. 10c). Ghosh et al.[182] introduced hygroscopic rare earth yttrium salts into PVDF to obtain porous piezoelectric composite membranes. The film exhibited excellent piezoelectric properties, which could be attributed to self-polarized –CH$_2$/–CF$_2$ dipoles. The open circuit voltage (V_{oc}) and short circuit current (I_{sc}) of the nanogenerator based on this composite film could reach 10 V and 63 μA, respectively. This material will play an increasingly significant role in the self-powered flexible electronics field. Using the solution casting method, Tamang et al.[183] incorporated condensed nanostructured DNA in PVDF to prepared a β-phase PVDF film, for which there was no need for later polarization processing. The maximum instantaneous output P of a nanogenerator based on this film was up to 11.5 μW cm^{-2}.

In addition to the aforementioned methods, some other methods have also been employed. Using a facile solvent evaporation method, Ghosh et al.[184] embedded Pt nanoparticles in P(VDF-HFP). This approach was time saving and simple facilities were needed. This film demonstrated excellent piezoelectric performance (d_{33} = −686 pm V^{-1}, P_r = 61.7 μC cm^{-2}, ε_r = 2678, and tan δ = 0.79).

12454 | *J. Mater. Chem. C*, 2018, **6**, 12446–12467

This journal is © The Royal Society of Chemistry 2018

Fu et al.[185] used a molten-salt synthetic method to prepared 600 nm sized BT nanoparticles which were modified with water-soluble polyvinylprrolidone (PVP). The BT/PVDF composite was prepared by mixing the BT nanoparticles and PVDF in solution, which was sequentially sonicated, evaporated, and hot pressed. The composite exhibited excellent piezoelectric properties ($\tan \delta$ = 0.02) and a high energy storage density (30×10^{-3} J cm^{-3}) under low electric fields.

2.2.2 Lead-free biopolymers. Some natural materials such as hydroxyapatite,[186] collagen fibrils[187] and cellulose[188] also exhibited piezoelectricity. These biomaterials have good biocompatibility and biodegradability. In addition, no harsh reaction conditions or complex reaction processes are required. Most importantly, these biomaterials are widely found in nature and have abundant sources.

Ghosh et al.[189] prepared light, flexible, and structurally stable gelatin nanofibers (GNF) by the electrospinning method from fish. The GNF displayed excellent mechanosensitivity (~ 0.8 V kPa^{-1}) and piezoelectric properties (d_{33} was around -20 pm V^{-1}). The self-powered electronic skin based on the GNF could be used for cutaneous pressure monitoring. In addition, Ghosh et al.[190,191] obtained bio-assembled chitin nanofibers and self-assembled collagen nanofibrils which were made from prawn shells and fish skin, respectively. These piezoelectric biomaterials could be employed to fabricate nanogenerators and piezoelectric sensors. Kim et al.[192] extracted a biodegradable chitin polymer which was also an excellent piezoelectric material from a squid pen. The chitin polymer was made into a chitin film by the spin casting method (Fig. 11) and the output current density of the chitin film based nanogenerator could reach 177 nA cm^{-2}. Maiti et al.[46] used bio-waste onion skin which was an efficient piezoelectric material without any chemical or surface treatment to prepare nanogenerators.

2.2.3 Other organic lead-free piezoelectric materials. In addition to the aforementioned biopolymers, some other natural materials (M13 bacteriophages, peptide nanotubes, etc.) also demonstrate promising piezoelectric properties. For instance, M13 bacteriophages were produced simply and economically by infecting bacteria, and they could produce a large number of new phage particles in a short period of time.[193] Lee et al.[194] not only validated the piezoelectricity of the phage fibers, but also improved the piezoelectric performance of the bacteriophages through DNA recombination technology to design a pVIII coating protein of the phages. d_{33} of these phages reached -7.8 pm V^{-1}. Shin et al.[195] prepared vertically aligned phage nanopillars (PNP) for which the height could be adjusted via an enforced infiltration method. Due to the unique vertically aligned structure, improved piezoelectric properties were obtained, and d_{33} reached -10.4 pm V^{-1}. Owing to the environmental friendliness and economic benefits, they had promising potential for self-powered implantable and wearable electronics applications.

Apart from M13 bacteriophages, peptide nanotubes were used as a piezoelectric material. Peptides have received widespread attention due to their biocompatibility, and unique biological and electronic properties.[196] Kholkin et al.[197] fabricated bioactive peptide nanotubes (PNT) which were self-assembled from peptide monomers of diphenylalanine. d_{33} of these PNT reached -60 pm V^{-1}. Besides, Nguyen et al.[198] prepared diphenylalanine peptide microrods and the polarization uniformity could be controlled by applying different electric fields. d_{33} of this material reached -17.9 pm V^{-1}, and the generator based on the peptide output a V_{oc} of 1.4 V and a P of 3.3 nW cm^{-2}. In short, this renewable and biocompatible biomaterial provides a new idea for the next generation of implantable multifunctional electronic devices.

Table 2 shows the preparation and some parameters of several organic lead-free piezoelectric materials. It is obvious that the piezoelectric properties of organic lead-free piezoelectric materials are relatively poor compared with those of inorganic
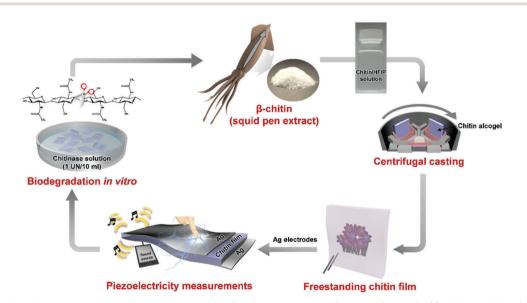

Fig. 11 The piezoelectricity measurements of biodegradable chitin film from a squid pen. Reprinted from ref. 192 with permission from Elsevier Ltd.

Table 2 A literature survey of the main parameters of organic lead-free piezoelectric materials

Category	Composition	Preparation method	d_{33} (pC N^{-1})	P_r (μC cm^{-2})	tan δ	Ref.
PVDF	β-Phase PVDF	Phase inversion technique	−49.6			155
	P(VDF-TrFE) nanowires	Template wetting method	35			163
	Yb-Doped PVDF	Solution casting process	−362.9	32.9	7.8	182
	Pt-Doped P(VDF-HFP)	Solvent evaporation method	−686	61.7	0.79	184
Biopolymers	Fish gelatin nanofibers	Electrospinning	−20			189
	Bio-assembled chitin nanofibers	Demineralization process	−2			190
	Self-assembled collagen nanofibrils	Descaling and demineralization process	−3		0.6	191
M13 bacteriophages	Phage fibers	DNA recombination technology	7.8			194
	Phage nanopillars	Enforced infiltration method	10.4			195
Peptide nanotubes	Bioactive peptide nanotubes	Self-assembly process	60			197
	Diphenylalanine peptide microrods	Self-assembly process	17.9			198

materials, but organic materials possess better flexibility and play an important role in fields such as wearable equipment, implantable equipment, *etc.*
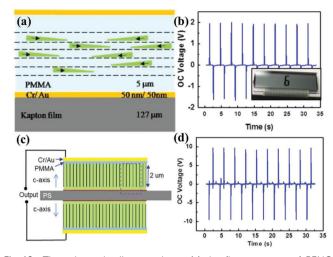
3. Recent advances in piezoelectric devices

With the development of new piezoelectric materials, innovative devices have been designed for versatile applications. For example, piezoelectric devices can generate and receive sound waves in water, and therefore are useful for underwater/geophysical exploration, sonic testing and so forth.[199,200] Smart piezoelectric devices are utilized to control the noise of aircraft and submarines.[201,202] In the field of optoelectronic information, piezoelectric materials are used for the manufacture of surface acoustic wave filters (SAWF), light shutters, optical waveguide modulators, optical displays and storage.[203–206] The following introduces piezoelectric devices including nanogenerators, sensors, and transducers using lead-free piezoelectric materials such as BaTiO$_3$, ZnO and PVDF polymer.

3.1 Piezoelectric nanogenerators (PENGs)

PENGs are micro generators which utilize the piezoelectric and semiconducting properties of piezoelectric materials to harvest the electricity generated by mechanical bending and compression. So far, PENGs have wide applications, for example, in wearable/implantable energy harvesters for detecting human health, in self-driven strain sensors in the field of human-computer interaction, in self-propelled chemical sensors to detect gas leaks, in self-charging batteries in the energy related field, *etc.*[207–210] Table 3 summaries the history of development of materials used for fabricating PENGs. The merits and shortcomings are listed as well.

3.1.1 ZnO-Based PENGs. Hu *et al.*[211] first designed two types of sandwich-structured PENGs with good mechanical stability and high performance utilizing ZnO nanowires (NWs). The first type of structure is shown in Fig. 12a, where a ZnO NW and dielectric mix was formed by spin-coating of a thin polymethyl methacrylate (PMMA) layer (100 nm) and dropping-on a solution containing conical-shaped ZnO NWs alternately several times, and then sandwiching between two Cr/Au films. A kapton film was used as the substrate in the NG.

Table 3 History of development of piezoelectric materials used for PENGs

Material	History	Merits	Defects
ZnO	Since 2006	Semiconducting properties; Biosafe and biocompatible; Nanostructure diversity	Low d_{33}; Poor mechanical properties
BaTiO$_3$	Since 2010	High d_{33}; High dielectric constant; Biocompatible	Low T_c; Difficult processing; Poor stability
PVDF and its composites	Since 2011	Low density; Excellent flexibility; Low impedance; Excellent chemical stability	Low d_{33}
Graphene	Since 2012	Excellent optical performance; Excellent mechanical properties	Low d_{33}; High cost
ZnSnO$_3$	Since 2012	Excellent piezoelectric properties; Non-toxic; Eco-friendly	Difficult synthesis; Poor mechanical properties
Biomaterials	Since 2014	Environment friendly; Cost-effective; Abundant	Poor piezoelectric properties

Fig. 12 The schematic diagram shows (a) the first structure of PENGs using ZnO NWs. (b) The V_{oc} of the PENG based on the first structure and the photograph of a LCD screen actuated by the PENG is shown in the inset. (c) The second structure of PENGs using ZnO NWs. (d) The V_{oc} of the PENG based on the second structure. Reproduced from ref. 211 with permission from Elsevier Ltd.

The V_{oc} of the PENG reached 2 V (Fig. 12b) and the I_{sc} exceeded 50 nA which could be calculated from eqn (1) and (2).

$$V_{oc} = \frac{I_{sc}g_{33}L}{4fd_{33}A} \quad (1)$$

$$I_{sc} = d_{33}YA\dot{\varepsilon} \quad (2)$$

where d_{33} is the piezoelectric constant, Y is Young's modulus, A is the effective contact area, $\dot{\varepsilon}$ is the applied strain rate, g_{33} is the voltage constant, L is the thickness and f is the average stimulating frequency.
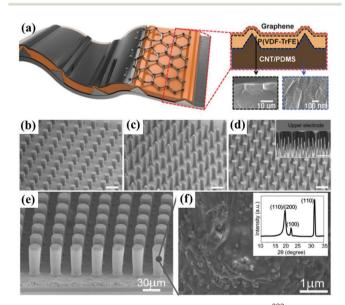
In the second type of structure (Fig. 12c), dense-packed ZnO NWs were grown on both sides of the polyester substrate *via* the hydrothermal method, and then a thin layer of PMMA was spin coated onto ZnO NW arrays for insulation, followed by deposition of a layer of Cr/Au that functioned as the electrode of the PENG. Finally, polydimethylsiloxane (PDMS) was used to completely wrap the entire device up to improve mechanical stability. The measured V_{oc} reached 10 V (Fig. 12d), and I_{sc} exceeded 0.6 μA.

However, the piezoelectric performance of ZnO-based PENGs is limited by the electron screening effect of n-type ZnO material, which results in a serious reduction in output voltage and current. Enormous efforts have been made to address this challenge.[212–214] Liu et al.[215] synthesized Cl-doped ZnO nanowires grown on a polyethylene terephthalate (PET) substrate by a modified hydrothermal method. A Cu layer (100 nm) was later sputtered on the top of the nanowires and the bottom of the PET to reduce the electron screening effect. The PENG output a maximum voltage and current of 4.9 V and 1030 nA, respectively. Yin et al.[216] employed a simple and low cost two-step method to fabricate a NiO–ZnO heterostructure. The p–n junction of NiO–ZnO suppressed electronic screen effects and therefore the

piezoelectric performance of the PENG was significantly improved. The output voltage of the PENG was 21 times of that of its counterpart based on ZnO. Similarly, Lu et al.[217] introduced Au particles to the surface of a ZnO nanoarray and the Schottky junctions of the Au@ZnO nanoarray remarkably reduced the electron screening effect.

3.1.2 PVDF-Based PENGs. Apart from ZnO, other piezoelectric materials for PENG applications have been developed, among which PVDF-based materials have been widely studied.[218–220] With their excellent flexibility, PVDF and its copolymers and their composites have been widely used in the field of flexible PENGs.

Karan et al.[221] demonstrated a novel flexible hybrid piezoelectric nanogenerator (HPNG) using PVDF and AlO–rGO (aluminum oxide decorated reduced graphene oxide) by a facile solution casting method. The device was able to harvest energy from both biomechanical and mechanical energy sources and output a V_{oc} of 36 V, an I_{sc} of 0.8 μA, and a maximum P of 27.97 μW cm^{-3}. The energy conversion efficiency reached up to 12.47%. This HPNG was promising for portable and flexible electronic devices. Utilizing both the piezoelectric and thermoelectric properties of P(VDF-TrFE), Lee et al.[222] proposed a piezoelectric–thermoelectric NG, that is, a hybrid stretchable nanogenerator (HSNG). The device mainly consisted of three layers, graphene nanosheets, the piezoelectric P(VDF-TrFE) with a micro-pattern structure, and micro-patterned polydimethylsiloxane–carbon nanotubes (PDMS–CNTs) as shown in Fig. 13a. Graphene served as the top flexible electrode, P(VDF-TrFE) served as a piezoelectric and thermoelectric material, and PDMS–CNT

Fig. 13 (a) The schematic illustration of the HSNG device.[222] SEM images of the composite at the (b) starting, (c) middle and (d) finish stage of the micropillar formation, the cross-section SEM image of the microfiber array is shown in the inset of (d). (e) SEM image of the P(VDF-TrFE)/BaTiO$_3$ nanocomposite micropillar array. (f) The magnified side-view SEM image of a nanocomposite micropillar and the XRD spectrum of the nanocomposite is shown in the inset.[225] Reproduced from ref. 222 and 225 with permission from John Wiley & Sons Ltd.

served as the bottom electrode that made the HSNG stretchable and flexible. High thermoelectric output was obtained when a thermal gradient was applied to the graphene side of the HSNG. The HSNG was believed to be suitable for wearable devices, robots and biomedical applications.

In order to enhance the performance of PVDF-based PENGs, piezoelectric composites were prepared. Siddiqui et al.[223] proposed a novel stretchable PENG consisting of a 3D micro-patterned PDMS substrate, two graphite electrodes and a stacked mat which was made up of a nanocomposite of BT nanoparticles/polyurethane (BT NPs-PU) and P(VDF-TrFE). The piezoelectric nanocomposite endowed the PENG with excellent piezoelectric properties while the 3D PDMS substrate provided sufficient stretchability, high stability and mechanical robustness under tension. The PENG output a V_{oc} of 10.1 V and a P of 1.76 μW cm^{-2} according to eqn (3):

$$P = \frac{1}{A} \times \frac{V_l^2}{R_l} \qquad (3)$$

where A is the effective contact area and V_l is the voltage drop across the load resistance R_l. No drop off in the output power of the PENG was observed after 9000 tensile cycles under 30% strain conditions, indicating the promising potential for applications in self-powered autonomous systems and wearable self-powered systems.

Another strategy to improve the piezoelectric performance is to design innovative microstructures. For instance, Chen et al.[224] used a P(VDF-TrFE) microfiber array (Fig. 13b–d) to fabricate a novel self-connected vertically integrated generator (SVIG). The output voltage and current could reach 4.0 V and 2.6 μA, which could be used for powering wireless mobile electronics. Chen et al.[225] proposed a novel flexible PENG based on (P(VDF-TrFE))/ BaTiO$_3$ nanocomposite micropillar arrays (Fig. 13e and f). This NG produced a maximum output voltage of 13.2 V and the average current density was up to 0.33 μA cm^{-2}. The high performance was ascribed to the enhanced piezoelectric properties of the nanocomposite and the excellent mechanical flexibility of the micropillar array.
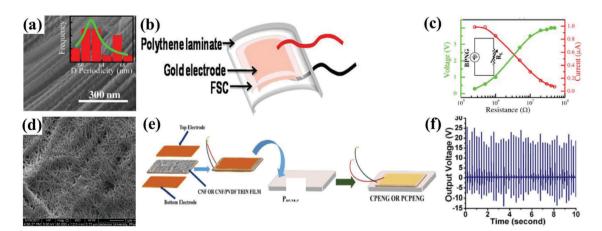
3.1.3 Biopolymer-based PENGs.
Eco-friendly, biocompatible and biodegradable bio-wastes such as fish skin, fish scales, fish maws, shrimp shell, etc. have been considered as ideal choices for fabrication of bio-piezoelectric nanogenerators (BPENGs).[226,227] The recycling of these bio-wastes into BPENGs not only reduces environmental pollution, but also proves to be a cost-effective approach to obtain high value products. Recently, Ghosh et al.[228] used fish scales (FSC) which were mainly composed of self-assembled and ordered collagen nano-fibrils to design a BPENG for biomedical sensor applications. Gold electrodes were sputtered on both sides of a fish scale, and then laminated with polypropylene (PP) to obtain the BPENG (Fig. 14a–c). The well-aligned nano-fibrils endowed the BPENG with superior piezoelectric performance and mechanical properties. I_{sc} and V_{oc} of the BPENG reached 1.5 μA and 4 V, respectively, and P reached as high as 1.14 μW cm^{-2}. Similarly, fish maws contained lots of collagen nano-fibrils, and therefore exhibited good piezoelectric performance.[229]

Chitin nanofibers are a biocompatible, non-toxic, renewable, biodegradable piezoelectric material which could be extracted from crab-shell by a simple mechanical process after removing the protein and minerals. V_{oc} and I_{sc} of the BPENG based chitin nanofibers (Fig. 14d–f) reported by Hoque et al.[230] reached 22 V and 0.12 μA, respectively. The BPENG also demonstrated excellent mechanical stability even after more than 10 000 cycles.

Table 4 shows the performance parameters (V_{oc} and I_{sc}) of PENGs presented in this paper. It is obvious that further work in terms of device optimization and synthesis of new advanced piezoelectric materials are critically important to improve the overall performance of PENGs to meet the demand of practical applications. Besides, standard approaches to study PENGs need to be well established and complete data is necessary to provide in published papers to better determine the merits of different results.

3.2 Piezoelectric sensors

The piezoelectric sensor, also called a vibration sensor, produces a voltage when a physical strain is applied.[231,232] Piezoelectric sensors

Fig. 14　(a) FESEM image of a fish scale with the histogram profile of D-periodicity in the inset. (b) The schematic diagram of the BPENG. (c) The variation of output voltage and current and the inset shows the corresponding equivalent circuit diagram. (d) FESEM micrograph of CNF. (e) Schematic image of device fabrication. (f) V_{oc} of the BPENG under continuous finger touch. Reprinted from ref. 228 with permission from AIP Publishing.

Table 4 Partial output performance data of PENGs in published papers

State	Piezoelectric material	Device structure	V_{oc} (V)	I_{sc} (nA)	P	Ref.
Normal	ZnO nanowires	Sandwich-structured	2	50		211
Normal	ZnO nanowires	Sandwich-structured	10	600		211
Flexible	Cl-Doped ZnO nanowires	Sandwich-structured	4.9	1030		215
Normal	NiO–ZnO heterostructure	Sandwich-structured	0.43	40		216
Hybrid flexible	PVDF/AlO–rGO	Sandwich-structured	36	0.8	27.97 µW cm^{-3}	221
Hybrid stretchable	P(VDF-TrFE)	Sandwich-structured	1.4			222
Stretchable	BT NPs-PU and P(VDF-TrFE)	Sandwich-structured	10.1		1.76 µW cm^{-2}	223
Self-connected vertically integrated	P(VDF-TrFE) microfibers	Sandwich-structured	4.0	2600		224
Flexible	(P(VDF-TrFE))/(BaTiO$_3$) nanocomposite micropillars	Sandwich-structured	13.2		12.7 µW cm^{-2}	225
Flexible	Collagen nano-fibrils	Sandwich-structured	4	1.5	1.14 µW cm^{-2}	228
Flexible	Chitin nanofibers	Sandwich-structured	22	0.12	97 µW cm^{-3}	230

have a wide range of applications. For example, piezoelectric sensors can be used to measure the vibration of a structure in the field of civil engineering,[233] to detect the speed of a car and the total weight of a body in the field of public transportation,[234] to examine human bodies in the medical domain,[235] and to inspect noise and to inspect gas leaks in the environmental field.[236,237]

Yu *et al.*[238] proposed a flexible piezoelectric tactile sensor array using PVDF film, which was used to measure the distribution of dynamic contact force along *X*-, *Y*-, and *Z*-axes. Arranged as 3 × 2 matrices, the sensor array consisted of six tactile units with an interval of 8 mm between adjacent units (Fig. 15a). Four piezoelectric capacitors were formed in each unit by sandwiching the PVDF film between four square-shaped upper electrodes and lower electrodes. In order to facilitate the force transmission, a trapezoid-shaped bump was placed above the four

angular piezoelectric capacitors (Fig. 15b–d). Charge changes occurred on four capacitors when a three-axis contact force was transmitted from the top of the bump, and the normal and shear components of the force could be calculated. The device worked with good linearity, low coupling effect and high repeatability, and it could even work under normal and shear loads ranging from 5 to 400 Hz. In addition, the sensor array could be easily integrated with uneven surfaces, for example, robotic and prosthetic hands, because of its good flexibility.

Based on PVDF film by inflation technology, Kim *et al.*[239] proposed a dome-shaped piezoelectric tactile sensor. Fig. 16a and b presents the conceptual view of the tactile sensor. A 4 × 4 dome-shaped cell, a polyimide film used for electrode protection, a bump structure, an Ag electrode layer, and a PDMS diaphragm used for supporting the sensor made up
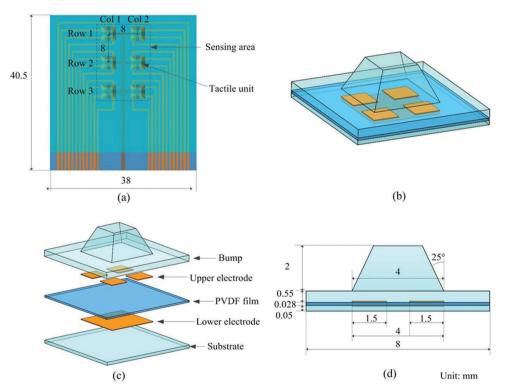

Fig. 15 Conceptual diagram of the proposed three-axis tactile sensor array. (a) Top view of the array. (b) Schematic view of a tactile unit. (c) Exploded view of a tactile unit, and (d) cross-sectional view of a tactile unit.

This journal is © The Royal Society of Chemistry 2018

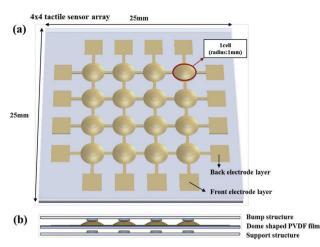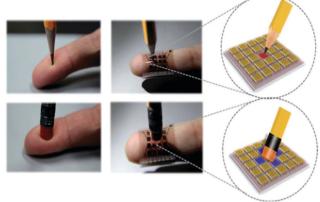J. Mater. Chem. C, 2018, 6, 12446–12467 | 12459

Fig. 16 The conceptual view of the piezoelectric tactile sensor array. (a) Front and (b) side view. Reproduced from ref. 239 with permission from Elsevier Ltd.

Fig. 18 Schematic diagram of how the piezoelectric tactile sensor produces an electrical 'pain' signal. The 'pain' or 'smooth' feeling signals was induced by the pressure levels and the distribution shape of activated cells.

the sensor module. The piezoelectric sensor converted an applied contact force to an electrical signal by the piezoelectric effect. When an external normal force was applied, a deformation of the cell was caused, and correspondingly, the device output a voltage which was proportional to the deformation. A higher sensitivity was obtained in this device with a dome structure than its traditional counterparts with a flat structure. This device was expected to have great potential in the field of robotic tactile sensors.

P(VDF-TrFE) has received a lot of attention for piezoelectric sensor applications. Compared to PVDF which usually needs to be polarized using complex equipment, P(VDF-TrFE) does not require complicated post-polarization treatment.[240] Using flexible (P(VDF-TrFE)) fiber arrays (Fig. 17a), Persano et al.[241] designed a vibration sensor (Fig. 17b). P(VDF-TrFe) aligned fiber arrays were placed upon kapton film, and then connected to copper film with silver paint on both ends. Due to the aligned structure and strongly preferential orientations, this device demonstrated excellent piezoelectric performance and could detect very small vibrations, which even had a high output voltage at low sound intensity (Fig. 17c).

ZnO has also been used in the field of piezoelectric tactile sensors. The sensor designed by Jeong et al.[242] using ZnO NW arrays had advantages of being self-powered, high resolution,

multi-touch, and simple design. The electrical power generated from the ZnO NWs rendered it easy to evaluate the pressure value. Meanwhile, the array design made it possible for the sensor to perceive the pressure level and the shape of the object (Fig. 18). Electrical "pain" warning signals would be generated when the device recognized that it was pricked by a sharp object with large force. Therefore, this design has promising potential for applications in the fields of electrical equipment and the robotic industry.

3.3 Piezoelectric transducers

A piezoelectric transducer is a device which converts acoustic energy, mechanical energy, electrical energy, etc. into another form of energy using piezoelectric materials.[243,244] Piezoelectric transducers play a significant role in many fields, especially in the field of energy, which collect sound, water, and kinetic energy in nature and convert them into electric energy.[245,246] In addition, piezoelectric transducers are also helpful for detecting underwater targets and natural disasters.[247] In order to meet the increasing demands, innovative piezoelectric transducers with advanced materials and structures are emerging.

Hu et al.[248] constructed a multilayer thin film structured $(Au/Co_3O_4/ZnO/Ti)$ piezoelectric transducer (Fig. 19a). In the transducer, the p–n junction formed at the Co_3O_4/ZnO interface increased the Fermi level difference between the two electrodes,
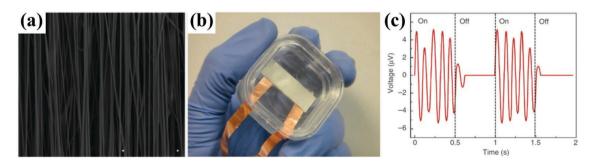

Fig. 17 (a) SEM image of P(VDF–TrFE) fiber arrays. (b) Photograph of the P(VDF–TrFe) nanofiber-based sensor. (c) The output voltage of the device in a 70 dB intensity. Reprinted from ref. 241 with permission from Macmillan Publishers Ltd.
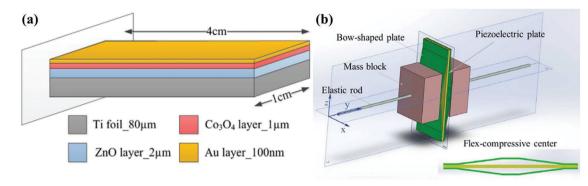
Fig. 19 (a) Co_3O_4/ZnO p–n type.[248] (b) Diagram of the MC-PEH. The enlarged view of the flex-compressive center is shown in the inset.[249] Reproduced from ref. 248 with permission from Elsevier Ltd and redrawn from ref. 249.

resulting in a dramatic increase in output power compared to that of ZnO piezoelectric transducers. For instance, at a low operating frequency of 37 Hz, the transducer output a power of 10.4 μW, much larger than that of a ZnO piezoelectric transducer (0.95 μW).

Yang et al.[249] designed a new multidirectional compressive mode piezoelectric energy harvester (MC-PEH). The proposed MC-PEH on a vibrating base had a symmetrical structure supported by two elastic rods. The main components included a pair of two mass blocks and a flex-compressive center which consisted of a piezoelectric plate (i.e. BT plate, KNN plate, BNT plate) and two bow-shaped metal plates (Fig. 19b). The flex-compressive center acted as the core part of this device. This device was similar to a cymbal transducer,[250] but this device had a rectangular section and only caused compressive force in the piezoelectric plate. The device was capable of scavenging inertial energy and the working frequency spectrum could be adjusted by adding damping blocks. In the meantime,

MC-PEH could effectively harvest the vibration energy along the Z-axis. In short, the MC-PEH output high voltage at a wide working bandwidth in the low frequency range, which had good application prospects in the future.

Jung et al.[29] demonstrated a flexible piezoelectric PVDF-based energy harvesting system for roadway applications. This energy harvester could collect the vibration energy over the road generated by a vehicle passing. As is shown in Fig. 20a, the device consisted of a nickel-based conductive tape (15 μm in thickness), a PVDF film (110 μm in thickness), and a polyimide substrate (300 μm in thickness). The energy output could be manipulated by adjusting the number of collectors connected in parallel which were then connected to rectifier and impedance matching circuit (Fig. 20b). At a speed of 8 km h^{-1} and a weight of 250 kgf, the unit harvester consisting of ten devices in parallel (Fig. 20c) output an instantaneous power up to 200 mW. This type of harvester could be used for large scale energy harvesting applications.
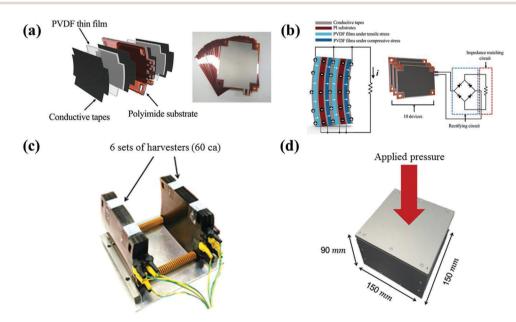

Fig. 20 (a) Schematic and image of the bi-morph structure energy harvester. (b) Parallel connection of unit harvesters. The stacked unit harvesters are then connected to a rectifying circuit and impedance matching circuit. (c) The interior and (d) exterior of the constructed energy harvester module. Reproduced from ref. 29 with permission from Elsevier.

Although it is of promising potential to harvest energy from the surrounding environment, harvesting low-frequency vibration energy remains a challenge. In this content, Huang et al.[251] designed an innovative beating type piezoelectric energy harvester based on microelectromechanical systems (MEMS) using PVDF. This energy harvester could collect low-frequency vibration energy with a high energy collection efficiency. To collect mechanical energy produced by human motion, Zhao et al.[252] fabricated a piezoelectric energy harvester that could be installed in a shoe. The energy harvester output an average power of 1 mW during a walk at a frequency of 5 Hz. This work proved the feasibility of energy harvesters for wearable device applications. Recently, energy harvesters with additional features were explored. Toprak et al.[253] demonstrated a microelectromechanical system (MEMS) scale cantilever-type piezoelectric energy harvester (PEH) based on P(VDF-TrFE) which had a P_r of 6.1 μC cm^{-2} and a coercive field of 74.9 V μm^{-1}. This harvester is suitable for manufacturing self-sustaining low-power electronic devices.

4. Conclusions and perspectives

This paper overviews the most recent advances in both inorganic and organic lead-free piezoelectric materials and state-of-the-art piezoelectric devices. Typical inorganic piezoelectric ceramics (i.e. BT-based, KNN-based, and BNT-based ceramic systems and BLSFs ceramics), ZnO nanostructures, and others such as ZnSnO$_3$ are reviewed. Organic PVDF and its polymers and their composites, as well as some biopolymers are summarized. State-of-the-art piezoelectric devices (i.e. nanogenerators, actuators, sensors, and transducers) are then presented. Lead-free piezoelectric materials are believed to replace lead-based piezoelectric materials in the future. Significant progress has been made to improve the piezoelectric performance of lead-free piezoelectric materials via the optimization of the preparation process and developing cutting-edge technologies. Based on these lead-free materials, piezoelectric devices have been designed. Nevertheless, there is still a long way to go for lead-free piezoelectric materials and their devices. For example, BT has good piezoelectric properties, but it is limited by a low Curie temperature. BNT has a higher Curie temperature, but its piezoelectric properties still need further improvement. KNN is difficult to process into dense ceramics by the conventional sintering method. BLSFs are hard to polarize which could enhance the piezoelectric properties. ZnO and ZnSnO$_3$ have a narrow application range and are limited to fabricating nanogenerators. The piezoelectric properties of PVDF and its copolymers are inferior to those of piezoelectric ceramics. Biopolymers also have relatively poor piezoelectric performance. Similarly, the high cost associated with lead-free piezoelectric devices and/or poor performance impose serious limitations on their practical applications. Therefore, it is imperative to develop high performance and cost-effective piezoelectric materials, and to optimize the design of piezoelectric devices.

Conflicts of interest

There are no conflicts to declare.

Acknowledgements

References

1 N. Viet, X. Xie, K. Liew, N. Banthia and Q. Wang, Energy, 2016, 112, 1219–1226.
2 X. Xie and Q. Wang, Energy, 2015, 86, 385–392.
3 E. Aksel and J. L. Jones, Sensors, 2010, 10, 1935–1954.
4 P. K. Panda, J. Mater. Sci., 2009, 44, 5049–5062.
5 M. H. Malakooti and H. A. Sodano, Appl. Phys. Lett., 2013, 102, 197–202.
6 S. Joshi, M. M. Nayak and K. Rajanna, Appl. Surf. Sci., 2014, 296, 169–176.
7 Y. Zhu, X. Zheng, L. Li, Y. Yu, X. Liu and J. Chen, Ferroelectrics, 2017, 520, 202–211.
8 L. Wei, Z. Xu, R. Chu, F. Peng and G. Zang, J. Am. Ceram. Soc., 2011, 94, 4131–4133.
9 T. Ogawa and Y. Numamoto, Jpn. J. Appl. Phys., 2002, 41, 7108–7112.
10 F. Z. Yao, K. Wang and J. F. Li, J. Appl. Phys., 2013, 113, 797–804.
11 D. Xu, X. Cheng, X. Guo and S. Huang, Constr. Build. Mater., 2015, 84, 219–223.
12 K. W. Kwok, H. L. W. Chan and C. L. Choy, IEEE Trans. Ultrason Ferroelectr. Freq. Control, 1997, 44, 733–742.
13 H. Jaffe, Piezoelectric Ceramics, Mullard, 1974.
14 G. Goodman, J. Am. Ceram. Soc., 1953, 36, 368–372.
15 B. Jaffe, R. S. Roth and S. Marzullo, J. Appl. Phys., 1954, 25, 809–810.
16 M. Yokosuka, Jpn. J. Appl. Phys., 1977, 16, 379–380.
17 R. J. Bouchard, L. H. Brixner and M. J. Popowich, US Pat., US4063341 A, 1977.
18 Q. Zhou, K. H. Lam, H. Zheng, W. Qiu and K. K. Shung, Prog. Mater. Sci., 2014, 66, 87–111.
19 Y. Lian, F. He, H. Wang and F. Tong, Biosens. Bioelectron., 2015, 65, 314–319.
20 S. Hirsch, J. Guo, R. Reiter, S. Papazoglou, T. Kroencke, J. Braun and I. Sack, Magn. Reson. Med., 2014, 71, 267–277.
21 B. Ju, W. Shao and Z. Feng, IEEE Trans. Power Electron., 2016, 31, 524–532.
22 B. G. Elmegreen, G. J. Martyna, D. M. Newns and A. G. Schrott, US9251884 B, 2017.
23 K.-I. Park, S. Xu, Y. Liu, G.-T. Hwang, S.-J. L. Kang, Z. L. Wang and K. J. Lee, Nano Lett., 2010, 10, 4939–4943.

24 K. I. Park, M. Lee, Y. Liu, S. Moon, G. T. Hwang, G. Zhu, J. E. Kim, S. O. Kim, D. K. Kim and Z. L. Wang, *Adv. Mater.*, 2012, **24**, 2999–3004.

25 S. H. Shin, Y. H. Kim, M. H. Lee, J. Y. Jung and J. Nah, *ACS Nano*, 2014, **8**, 2766–2773.

26 H. Gullapalli, V. S. Vemuru, A. Kumar, A. Botello-Mendez, R. Vajtai, M. Terrones, S. Nagarajaiah and P. M. Ajayan, *Small*, 2010, **6**, 1641–1646.

27 R. Agrawal and H. D. Espinosa, *Nano Lett.*, 2011, **11**, 786–790.

28 B. Kumar and S.-W. Kim, *Nano Energy*, 2012, **1**, 342–355.

29 (*a*) I. Jung, Y. H. Shin, S. Kim, J. Y. Choi and C. Y. Kang, *Appl. Energy*, 2017, **197**, 222–229; (*b*) H. Liu, M. Dong, W. Huang, J. Gao, K. Dai, J. Guo, G. Zheng, C. Liu, C. Shen and Z. Guo, *J. Mater. Chem. C*, 2017, **5**, 73–83; (*c*) S. M. Aqeel, Z. Huang, J. Walton, C. Baker, D. Falkner, Z. Liu and Z. Wang, *Adv. Compos. Hybrid Mater.*, 2018, **1**, 185–192; (*d*) E. Ghafari, X. Jiang and N. Lu, *Adv. Compos. Hybrid Mater.*, 2018, **1**, 332–340.

30 S. R. Khaled, D. Sameoto and S. Evoy, *Smart Mater. Struct.*, 2014, **23**, 033001.

31 M. A. Hannan, S. Mutashar, S. A. Samad and A. Hussain, *BioMed. Eng. OnLine*, 2014, **13**, 79–101.

32 A. E. N. N. Abd-Alla and N. A. Askar, *Appl. Math. Inform. Sci.*, 2014, **8**, 1625–1632.

33 F. Wang, X. Min, Y. Tang, W. Tao, W. Shi and C. M. Leung, *J. Am. Ceram. Soc.*, 2012, **95**, 1955–1959.

34 F. F. Ru, T. Wei and W. Z. Lin, *Adv. Mater.*, 2016, **28**, 4283–4305.

35 X. Li and E. C. Kan, *Sens. Actuators, A*, 2011, **163**, 457–463.

36 Y. W. Song, S. Y. Lee, J. Y. Lee, J. A. Lim, J. W. Choi, B. K. Cheong, J. S. Kim, H. S. Jang and H. J. Yi, US20150201837, 2015.

37 P. Panda and B. Sahoo, *Ferroelectrics*, 2015, **474**, 128–143.

38 C. R. Bowen, H. A. Kim, P. M. Weaver and S. Dunn, *Energy Environ. Sci.*, 2013, **7**, 25–44.

39 I. T. Seo, C. H. Choi, D. Song, M. S. Jang, B. Y. Kim, S. Nahm, Y. S. Kim, T. H. Sung and H. C. Song, *J. Am. Ceram. Soc.*, 2013, **96**, 1024–1028.

40 T. R. Shrout and S. J. Zhang, *J. Electroceram.*, 2007, **19**, 113–126.

41 T. Takenaka, K.-i. Maruyama and K. Sakata, *Jpn. J. Appl. Phys.*, 1991, **30**, 2236–2239.

42 S.-H. Park, C.-W. Ahn, S. Nahm and J.-S. Song, *Jpn. J. Appl. Phys.*, 2004, **43**, L1072–L1074.

43 T. Takenaka and H. Nagata, *J. Eur. Ceram. Soc.*, 2005, **25**, 2693–2700.

44 D. Lin, D. Xiao, J. Zhu, P. Yu, H. Yan and L. Li, *Mater. Lett.*, 2004, **58**, 615–618.

45 S. K. Karan, D. Mandal and B. B. Khatua, *Nanoscale*, 2015, **7**, 10655–10666.

46 S. Maiti, S. K. Karan, J. Lee, A. K. Mishra, B. B. Khatua and J. K. Kim, *Nano Energy*, 2017, **42**, 282–293.

47 M. Yasseri, H. Abdizadeh, A. Shakeri and M. R. Golobostanfard, *Adv. Mater. Res.*, 2013, **829**, 727–731.

48 K. Uchino, E. Sadanaga and T. Hirose, *J. Am. Ceram. Soc.*, 1989, **72**, 1555–1558.

49 N. Novak, R. Pirc and Z. Kutnjak, *Phys. Rev. B: Condens. Matter Mater. Phys.*, 2013, **87**, 104102.

50 R. R. Mcquade and M. R. Dolgos, *J. Solid State Chem.*, 2016, **242**, 140–147.

51 Z. Sun, L. Zhang, F. Dang, Y. Liu, Z. Fei, Q. Shao, H. Lin, J. Guo, L. Xiang and N. Yerra, *CrystEngComm*, 2017, **19**, 1–34.

52 J. P. Praveen, T. Karthik, A. James, E. Chandrakala, S. Asthana and D. Das, *J. Eur. Ceram. Soc.*, 2015, **35**, 1785–1798.

53 J. I. Roscow, R. W. C. Lewis, J. Taylor and C. R. Bowen, *Acta Mater.*, 2017, **128**, 207–217.

54 L. Zhang, M. Zhang, L. Wang, C. Zhou, Z. Zhang, Y. Yao, L. Zhang, D. Xue, X. Lou and X. Ren, *Appl. Phys. Lett.*, 2014, **105**, 162908.

55 L. M. Denis, J. Glaum, M. Hoffman, J. E. Daniels, R. J. Hooper, G. Tutuncu, J. S. Forrester and J. L. Jones, *J. Mater. Sci.*, 2018, **53**, 1672–1679.

56 I. Coondoo, N. Panwar, H. Amorín, E. Ramana Venkata, M. Algueró and A. Kholkin, *J. Am. Ceram. Soc.*, 2015, **98**, 3127–3135.

57 C. Xu, Z. Yao, K. Lu, H. Hao, Z. Yu, M. Cao and H. Liu, *Ceram. Int.*, 2016, **42**, 16109–16115.

58 L.-F. Zhu, B.-P. Zhang, S. Li, L. Zhao, N. Wang and X.-C. Shi, *J. Alloys Compd.*, 2016, **664**, 602–608.

59 K.-I. Park, M. Lee, Y. Liu, S. Moon, G.-T. Hwang, G. Zhu, J. E. Kim, S. O. Kim, D. K. Kim, Z. L. Wang and K. J. Lee, *Adv. Mater.*, 2012, **24**, 2999–3004.

60 Y. Zhao, Q. Liao, G. Zhang, Z. Zhang, Q. Liang, X. Liao and Y. Zhang, *Nano Energy*, 2015, **11**, 719–727.

61 S. H. Shin, Y. H. Kim, H. L. Min, J. Y. Jung and J. Nah, *ACS Nano*, 2014, **8**, 2766–2773.

62 S. M. Keshk, *J. Bioprocess. Biotech.*, 2014, **4**, 150–159.

63 L. Hu, G. Zheng, J. Yao, N. Liu, B. Weil, M. Eskilsson, E. Karabulut, Z. Ruan, S. Fan and J. T. Bloking, *Energy Environ. Sci.*, 2013, **6**, 513–518.

64 S. C. Fernandes, P. Sadocco, A. Alonso-Varona, T. Palomares, A. Eceiza, A. J. Silvestre, I. A. Mondragon and C. S. Freire, *ACS Appl. Mater. Interfaces*, 2013, **5**, 3290–3297.

65 G. Zhang, Q. Liao, Z. Zhang, Q. Liang, Y. Zhao, X. Zheng and Y. Zhang, *Adv. Sci.*, 2016, **3**, 1500257.

66 X. Wang, J. Wu, D. Xiao, J. Zhu, X. Cheng, T. Zheng, B. Zhang, X. Lou and X. Wang, *J. Am. Chem. Soc.*, 2014, **136**, 2905–2910.

67 L. Egerton and D. M. Dillon, *J. Am. Ceram. Soc.*, 1959, **42**, 438–442.

68 J. Hreščak, B. Malič, J. Cilenšek and A. Benčan, *J. Therm. Anal. Calorim.*, 2017, **127**, 129–136.

69 C.-W. Ahn, H.-Y. Lee, G. Han, S. Zhang, S.-Y. Choi, J.-J. Choi, J.-W. Kim, W.-H. Yoon, J.-H. Choi, D.-S. Park, B.-D. Hahn and J. Ryu, *Sci. Rep.*, 2015, **5**, 17656–17663.

70 S. Bai, J. Zhang, Z. Chen, Y. Wang, L. Dong, C. Chen, Y. Yan and M. Hong, *Ceram. Int.*, 2018, **44**, 9794–9800.

71 J. Yang, F. Zhang, Q. Yang, Z. Liu, Y. Li, Y. Liu and Q. Zhang, *Appl. Phys. Lett.*, 2016, **108**, 182904.

72 B. Zhang, J. Wu, X. Cheng, X. Wang, D. Xiao, J. Zhu, X. Wang and X. Lou, *ACS Appl. Mater. Interfaces*, 2013, **5**, 7718–7725.

73 D. Lin, K. Kwok and H. Chan, *J. Alloys Compd.*, 2008, **461**, 273–278.

74 F. Rubio-Marcos, J. Romero, M. Martín-Gonzalez and J. Fernández, *J. Eur. Ceram. Soc.*, 2010, **30**, 2763–2771.

75 T. Men, F. Yao, Z. Zhu, K. Wang and J. Li, *J. Adv. Dielectr.*, 2016, **6**, 1650013.

76 Y. Su, X. Chen, H. Lian and J. Peng, *J. Mater. Sci.*, 2017, **52**, 2934–2943.

77 M. R. Bafandeh, R. Gharahkhani, M. H. Abbasi, A. Saidi, J.-S. Lee and H.-S. Han, *J. Electroceram.*, 2014, **33**, 128–133.

78 H. Du, Z. Li, F. Tang, S. Qu, Z. Pei and W. Zhou, *Mater. Sci. Eng., B*, 2006, **131**, 83–87.

79 J. Li, K. Wang, B. Zhang and L. Zhang, *J. Am. Ceram. Soc.*, 2006, **89**, 706–709.

80 C. A. Souza, J. A. Eiras and M. H. Lente, *Ferroelectrics*, 2016, **499**, 47–56.

81 D. Yang, C. Ma, Z. Yang, L. Wei, X. Chao, Z. Yang and J. Yang, *Ceram. Int.*, 2016, **42**, 4648–4657.

82 M. Feizpour, H. Barzegar Bafrooei, R. Hayati and T. Ebadzadeh, *Ceram. Int.*, 2014, **40**, 871–877.

83 T. Zheng, J. Wu, D. Xiao and J. Zhu, *Prog. Mater. Sci.*, 2018, 552–624.

84 F. Xu, S. Trolier-Mckinstry, W. Ren and B. Xu, *J. Appl. Phys.*, 2001, **89**, 1336–1348.

85 D. Lin, S. Zhang, C. Cai and W. Liu, *J. Appl. Phys.*, 2015, **117**, 113–126.

86 L. Zheng, X. Huo, R. Wang, J. Wang, W. Jiang and W. Cao, *CrystEngComm*, 2013, **15**, 7718–7722.

87 E. Hollenstein, M. Davis, D. Damjanovic and N. Setter, *Appl. Phys. Lett.*, 2005, **87**, 182905.

88 Y. Li, W. Chen, J. Zhou, Q. Xu, H. Sun and R. Xu, *Mater. Sci. Eng., B*, 2004, **112**, 5–9.

89 C. Jiang, X. Zhou, K. Zhou, M. Wu and D. Zhang, *Ceram. Int.*, 2017, **43**, 11274–11280.

90 L. Zheng, X. Yi, S. Zhang, W. Jiang, B. Yang, R. Zhang and W. Cao, *Appl. Phys. Lett.*, 2013, **103**, 3683–3685.

91 S. Xue, J. Ma, X. Zhao, F. Wang, D. Sun, T. Wang, W. Shi, Z. Fu, H. Zhou and H. Luo, *Appl. Phys. Lett.*, 2017, **111**, 162902.

92 W. Bai, J. Xi, J. Zhang, B. Shen, J. Zhai and H. Yan, *J. Eur. Ceram. Soc.*, 2015, **35**, 2489–2499.

93 P. Li, B. Liu, B. Shen, J. Zhai, L. Li and H. Zeng, *Ceram. Int.*, 2017, **43**, 1008–1021.

94 P. Dengfeng, W. Xusheng, X. Chaonan, Y. Xi, L. Jian and S. Tiantuo, *J. Am. Ceram. Soc.*, 2013, **96**, 184–190.

95 M. D. Maeder, D. Damjanovic and N. Setter, *J. Electroceram.*, 2004, **13**, 385–392.

96 B. Jaffe, *Piezoelectric Ceramics*, Elsevier, 2012.

97 E. C. Subbarao, *J. Phys. Chem. Solids*, 1962, **23**, 665–676.

98 C. M. Wang, J. F. Wang, C. Mao, X. Chen, X. Dong, Z. G. Gai and M. L. Zhao, *J. Am. Ceram. Soc.*, 2008, **91**, 3094–3097.

99 C. Diao, H. Zheng, L. Fang, Y. Gu and W. Zhang, *Ceram. Int.*, 2013, **39**, 6991–6995.

100 D. Peng, X. Wang, C. Xu, X. Yao, J. Lin and T. Sun, *J. Am. Ceram. Soc.*, 2013, **96**, 184–190.

101 Z. Shen, H. Sun, Y. Tang, Y. Li and S. Zhang, *Mater. Res. Bull.*, 2015, **63**, 129–133.

102 D. Hall, *J. Mater. Sci.*, 2001, **36**, 4575–4601.

103 G. C. C. da Costa, A. Z. Simões, A. Ries, C. R. Foschini, M. A. Zaghete and J. A. Varela, *Mater. Lett.*, 2004, **58**, 1709–1714.

104 A. Khokhar, M. L. V. Mahesh, A. R. James, P. K. Goyal and K. Sreenivas, *J. Alloys Compd.*, 2013, **581**, 150–159.

105 J. Rödel, W. Jo, K. T. P. Seifert, E. M. Anton, T. Granzow and D. Damjanovic, *J. Am. Ceram. Soc.*, 2010, **92**, 1153–1177.

106 P. Xiao, Y. Guo, M. Tian, Q. Zheng, N. Jiang, X. Wu, Z. Xia and D. Lin, *Dalton Trans.*, 2015, **44**, 17366–17380.

107 T. Ikeda, *Piezoelectricity*, Oxford University Press, Oxford, 1990.

108 Y. Lai, M. Meng, Y. Yu, X. Wang and T. Ding, *Appl. Catal., B*, 2011, **105**, 335–345.

109 X. Fang, J. Liu and V. Gupta, *Nanoscale*, 2013, **5**, 1716–1726.

110 A. Singh, *Adv. Powder Technol.*, 2010, **21**, 609–613.

111 D. Sharma, J. Rajput, B. Kaith, M. Kaur and S. Sharma, *Thin Solid Films*, 2010, **519**, 1224–1229.

112 M. Gupta, N. Sinha, B. K. Singh, N. Singh, K. Kumar and B. Kumar, *Mater. Lett.*, 2009, **63**, 1910–1913.

113 X. Wang, J. Song and Z. L. Wang, *J. Mater. Chem.*, 2007, **17**, 711–720.

114 N.-F. Hsu, T.-K. Chung, M. Chang and H.-J. Chen, *J. Mater. Sci. Technol.*, 2013, **29**, 893–897.

115 E. S. Nour, A. Echresh, X. Liu, E. Broitman, M. Willander and O. Nur, *AIP Adv.*, 2015, **5**, 077163.

116 X. Li, Y. Yang, X. Wu, F. C. Zhang and H. Yang, *Ferroelectrics*, 2018, **530**, 11–16.

117 Z. Zhao, N. Wang, H. Nan, L. Shen, C. Durkan and X. He, *J. Mater. Chem. C*, 2016, **4**, 5814–5821.

118 X. Wang, F. Sun, Y. Huang, Y. Duan and Z. Yin, *Chem. Commun.*, 2015, **51**, 3117–3120.

119 G. D. Jones, R. A. Assink, T. R. Dargaville, P. M. Chaplya, R. L. Clough, J. M. Elliott, J. W. Martin, D. M. Mowery and M. C. Celina, *J. Electron. Packag.*, 2005, **131**, 51–55.

120 R. Bhunia, S. Das, S. Dalui, S. Hussain, R. Paul, R. Bhar and A. K. Pal, *Appl. Phys. A: Mater. Sci. Process.*, 2016, **122**, 1–13.

121 K. Matsuo, R. J. Xie, Y. Akimune and T. Sugiyama, *J. Ceram. Soc. Jpn.*, 2002, **110**, 491–494.

122 J. M. Wu, C. Xu, Y. Zhang and Z. L. Wang, *ACS Nano*, 2012, **6**, 4335–4340.

123 M. M. Alam, S. K. Ghosh, A. Sultana and D. Mandal, *Nanotechnology*, 2015, **26**, 165403.

124 K. S. Ramadan, D. Sameoto and S. Evoy, *Smart Mater. Struct.*, 2014, **23**, 33001–33026.

125 A. Petchsuk, W. Supmak and A. Thanaboonsombut, *J. Am. Ceram. Soc.*, 2011, **94**, 2126–2134.

126 Q. Lu, L. Liu, X. Lan, Y. Liu and J. Leng, *Compos. Struct.*, 2016, **153**, 843–850.

127 X. Cui, X. Ni and Y. Zhang, *J. Alloys Compd.*, 2016, **675**, 306–310.

128 U. Now, T. R. L. Size and U. Recharging, *Adv. Mater. Sci. Eng.*, 2015, **2015**, 165631.

129 A. Mohebbi, F. Mighri, A. Ajji and D. Rodrigue, *Adv. Polym. Technol.*, 2016, 21686–21701.

12464 | *J. Mater. Chem. C*, 2018, **6**, 12446–12467

This journal is © The Royal Society of Chemistry 2018

130 Y. S. Rim, S. H. Bae, H. Chen, M. N. De and Y. Yang, *Adv. Mater.*, 2016, **28**, 4415–4440.

131 A. Decharat, S. Wagle and F. Melandsø, *Jpn. J. Appl. Phys.*, 2014, **53**, 05–16.

132 G. Harvey, A. Gachagan and T. Mutasa, *IEEE Trans. Ultrason Ferroelectr. Freq. Control*, 2014, **61**, 481–495.

133 J. Bernal-Martínez, A. Seseña-Rubfiaro, R. Godínez-Fernández and A. Aguilar-Elguezabal, *Microelectron. Eng.*, 2016, **166**, 10–14.

134 A. K. Batra, M. E. Edwards, P. Guggilla, M. D. Aggarwal and R. B. Lal, *Integr. Ferroelectr.*, 2014, **158**, 98–107.

135 J. Harrison and Z. Ounaies, *Piezoelectric Polymers*, Wiley Online Library, 2002.

136 S. Jana, S. Garain, S. Sen and D. Mandal, *Phys. Chem. Chem. Phys.*, 2015, **17**, 17429–17436.

137 A. Gasmi, C. Lewa and S. Łętowski, *Mater. Lett.*, 1992, **13**, 346–351.

138 A. G. Holmes-Siedle, P. D. Wilson and A. P. Verrall, *Mater. Des.*, 1983, **4**, 910–918.

139 C. Chang, V. H. Tran, J. Wang, Y. K. Fuh and L. Lin, *Nano Lett.*, 2010, **10**, 726–731.

140 A. Walther, M. Hoffmann and A. H. Müller, *Angew. Chem.*, 2008, **120**, 723–726.

141 O. Misoon and K. Seok, *Electrochim. Acta*, 2012, **59**, 196–201.

142 A. Bottino, G. Capannelli and A. Comite, *Desalination*, 2002, **146**, 35–40.

143 Y. Lee, J. Rho and B. Jung, *J. Appl. Polym. Sci.*, 2003, **89**, 2058–2067.

144 S. Chen, X. Tao, W. Zeng, B. Yang and S. Shang, *Adv. Energy Mater.*, 2017, **7**, 1601569.

145 K. Maity, B. Mahanty, T. K. Sinha, S. Garain, A. Biswas, S. K. Ghosh, S. Manna, S. K. Ray and D. Mandal, *Energy Technol.*, 2017, **5**, 234–243.

146 F. Mokhtari, M. Shamshirsaz and M. Latifi, *Polym. Eng. Sci.*, 2016, **56**, 61–70.

147 Y. Mao, P. Zhao, G. Mcconohy, H. Yang, Y. Tong and X. Wang, *Adv. Energy Mater.*, 2014, **4**, 1301624.

148 K. T. Lau, M. H. R. Ab Razak, S. L. Kok, M. Zaimi, M. W. Abd Rashid, N. Mohamad and M. A. Azam, *Appl. Mech. Mater.*, 2015, **761**, 412–416.

149 L. Dong, R. Li, C. Xiong and H. Quan, *Polym. Int.*, 2010, **59**, 756–758.

150 A. Jain, K. J. Prashanth, A. K. Sharma, A. Jain and P. N. Rashmi, *Polym. Eng. Sci.*, 2015, **55**, 1589–1616.

151 V. Tiwari and G. Srivastava, *J. Polym. Res.*, 2014, **21**, 587–594.

152 K. Ke, P. Pötschke, D. Jehnichen, D. Fischer and B. Voit, *Polymer*, 2014, **55**, 611–619.

153 P. Thakur, A. Kool, B. Bagchi, S. Das and P. Nandy, *Appl. Clay Sci.*, 2014, **99**, 149–159.

154 M. Sharma, G. Madras and S. Bose, *Phys. Chem. Chem. Phys.*, 2014, **16**, 14792–14799.

155 N. Soin, D. Boyer, K. Prashanthi, S. Sharma, A. A. Narasimulu, J. Luo, T. H. Shah, E. Siores and T. Thundat, *Chem. Commun.*, 2015, **51**, 8257–8260.

156 M. F. Kemmere, *Supercritical Carbon Dioxide: in Polymer Reaction Engineering*, 2005.

157 M. Howe-Grant, *Fluorine Chemistry: a Comprehensive Treatment*, Wiley & Sons, 1995.

158 S. Wolff, F. Jirasek, S. Beuermann and M. Türk, *RSC Adv.*, 2015, **5**, 66644–66649.

159 (a) P. Adhikary, S. Garain and D. Mandal, *Phys. Chem. Chem. Phys.*, 2015, **17**, 7275–7281; (b) S. Angaiah, V. Murugadoss, S. Arunachalam and S. Krishnan, *Eng. Sci.*, 2018, DOI: 10.30919/es8d756.

160 J. H. Lee, H. J. Yoon, T. Y. Kim, M. K. Gupta, J. H. Lee, W. Seung, H. Ryu and S. W. Kim, *Adv. Funct. Mater.*, 2015, **25**, 3203–3209.

161 E. Bolbasov, K. S. Stankevich, E. Sudarev, V. Bouznik, V. Kudryavtseva, L. Antonova, V. Matveeva, Y. G. Anissimov and S. Tverdokhlebov, *Mater. Chem. Phys.*, 2016, **182**, 338–346.

162 V. Strashilov, G. Alexieva, B. Vincent, V. Nguyen and D. Rouxel, *Appl. Phys. A: Mater. Sci. Process.*, 2015, **118**, 1469–1477.

163 R. A. Whiter, V. Narayan and S. Kar-Narayan, *Adv. Energy Mater.*, 2014, **4**, 1400519.

164 R. E. Newnham, D. P. Skinner and L. E. Cross, *Mater. Res. Bull.*, 1978, **13**, 525–536.

165 N. Jaitanong, R. Yimnirun, H. R. Zeng, G. R. Li, Q. R. Yin and A. Chaipanich, *Mater. Lett.*, 2014, **130**, 146–149.

166 C. David, J. F. Capsal, L. Laffont, E. Dantras and C. Lacabanne, *J. Phys. D: Appl. Phys.*, 2013, **45**, 415305.

167 H. Khanbareh, S. van der Zwaag and W. A. Groen, *Smart Mater. Struct.*, 2014, **23**, 64–75.

168 S. Mamada, N. Yaguchi, M. Hansaka, M. Yamato and H. Yoshida, *J. Appl. Polym. Sci.*, 2015, **132**, 45–51.

169 G. Gao, Q. Zhang and C. D. Vecitis, *J. Mater. Chem. A*, 2014, **2**, 6185–6190.

170 M. M. Abolhasani, K. Shirvanimoghaddam and M. Naebe, *Compos. Sci. Technol.*, 2017, **138**, 49–56.

171 U. Yaqoob, A. S. M. I. Uddin and G.-S. Chung, *Appl. Surf. Sci.*, 2017, **405**, 420–426.

172 H.-Q. Liang, Q.-Y. Wu, L.-S. Wan, X.-J. Huang and Z.-K. Xu, *J. Membr. Sci.*, 2014, **465**, 56–67.

173 A. Md Mehebub, S. Ayesha, S. Debabrata and M. Dipankar, *Nanotechnology*, 2017, **28**, 365401.

174 E.-J. Lee, A. K. An, P. Hadi, S. Lee, Y. C. Woo and H. K. Shon, *J. Membr. Sci.*, 2017, **524**, 712–720.

175 X. Huang, J. Zhang, W. Wang, Y. Liu, Z. Zhang, L. Li and W. Fan, *RSC Adv.*, 2015, **5**, 18258–18266.

176 (a) J. P. Jung, J.-S. Kim, T.-S. Han and J. H. Kim, *Macromol. Res.*, 2017, **25**, 365–373; (b) H. Liu, Y. Li, K. Dai, G. Zheng, C. Liu, C. Shen, X. Yan, J. Guo and Z. Guo, *J. Mater. Chem. C*, 2016, **4**, 157–166; (c) H. Liu, W. Huang, X. Yang, K. Dai, G. Zheng, C. Liu, C. Shen, X. Yan, J. Guo and Z. Guo, *J. Mater. Chem. C*, 2016, **4**, 4459–4469; (d) Y. Lu, M. C. Biswas, Z. Guo, J. Jeon and E. K. Wujcik, *Biosens. Bioelectron.*, 2019, **123**, 167–177; (e) H. Liu, J. Gao, W. Huang, K. Dai, G. Zheng, C. Liu, C. Shen, X. Yan, J. Guo and Z. Guo, *Nanoscale*, 2016, **8**, 12977–12989; (f) C. Hu, Z. Li, J. Gao, K. Dai, G. Zheng, C. Liu, C. Shen,

H. Song and Z. Guo, *J. Mater. Chem. C*, 2017, **5**, 2318–2328; (*g*) S. Zhao, G. Li, H. Liu, K. Dai, G. Zheng, X. Yan, C. Liu, J. Chen, C. Shen and Z. Guo, *Adv. Mater. Interfaces*, 2017, **4**, 1700265.

177 (*a*) M. Rawat and K. L. Yadav, *J. Polym. Res.*, 2015, **22**, 230–236; (*b*) C. Wang, Y. Wu, Y. Li, Q. Shao, X. Yan, C. Han, Z. Wang, Z. Liu and Z. Guo, *Polym. Adv. Technol.*, 2018, **29**, 668–676; (*c*) W. Yang, X. Wang, J. Li, X. Yan, S. Ge, S. Tadakamalla and Z. Guo, *Polym. Eng. Sci.*, 2018, **58**, 1127–1134; (*d*) C. Wang, B. Mo, Z. He, Q. Shao, D. Pan, E. Wujick, J. Guo, X. Xie, X. Xie and Z. Guo, *J. Membr. Sci.*, 2018, **556**, 118–125; (*e*) Y. Zhang, M. Zhao, J. Zhang, Q. Shao, J. Li, H. Li, B. Lin, M. Yu, S. Chen and Z. Guo, *J. Polym. Res.*, 2018, **25**, 130; (*f*) Y. Kong, Y. Li, G. Hu, J. Lin, D. Pan, D. Dong, E. Wujick, Q. Shao, M. Wu, J. Zhao and Z. Guo, *Polymer*, 2018, **145**, 232–241; (*g*) X. Wu, J. Song, J. Li, Q. Shao, N. Cao, N. Lu and Z. Guo, *Polymer*, 2017, **124**, 41–47; (*h*) Y. Kong, Y. Li, G. Hu, N. Cao, Y. Ling, D. Pan, Q. Shao and Z. Guo, *Polym. Adv. Technol.*, 2018, **29**, 2344–2351.

178 (*a*) R. Li, Z. Zhao, Z. Chen and J. Pei, *Mater. Express*, 2017, **7**, 536–540; (*b*) Y. Pan, D. W. Schubert, J. Ryu, E. Wujick, C. Liu, C. Shen and X. Liu, *Eng. Sci.*, 2018, **1**, 86–94; (*c*) X. Zhang, X. Wang, X. Liu, J. Lv, Y. Wang, G. Zheng, H. Liu, C. Liu, Z. Guo and C. Shen, *ACS Sustainable Chem. Eng.*, 2018, **6**, 12580–12585; (*d*) Z. Li, B. Wang, X. Qin, Y. Wang, C. Liu, Q. Shao, N. Wang, J. Zhang, Z. Wang, C. Shen and Z. Guo, *ACS Sustainable Chem. Eng.*, 2018, DOI: 10.1021/acssuschemeng.8b01637; (*e*) Z. Hu, D. Zhang, F. Lu, W. Yuan, X. Xu, Q. Zhang, H. Liu, Q. Shao, Z. Guo and Y. Huang, *Macromolecules*, 2018, **51**, 5294–5303; (*f*) M. Dong, Q. Li, H. Liu, C. Liu, E. Wujcik, Q. Shao, T. Ding, X. Mai, C. Shen and Z. Guo, *Polymer*, 2018, DOI: 10.1016/j.polymer.2018.11.003; (*g*) Z. Wu, S. Gao, L. Chen, D. Jiang, Q. Shao, B. Zhang, Z. Zhai, C. Wang, M. Zhao, Y. Ma, X. Zhang, L. Weng, M. Zhang and Z. Guo, *Macromol. Chem. Phys.*, 2017, **218**, 1700357; (*h*) C. Wang, B. Mo, Z. He, C. X. Zhao, L. Zhang, Q. Shao, X. Guo, E. Wujcik and Z. Guo, *Polymer*, 2018, **138**, 363–368; (*i*) Y. Li, T. Jing, G. Xu, J. Tian, M. Dong, Q. Shao, B. Wang, Z. Wang, Y. Zheng, C. Yang and Z. Guo, *Polymer*, 2018, **149**, 13–22; (*j*) X. Cui, G. Zhu, Y. Pan, Q. Shao, C. Zhao, M. Dong, Y. Zhang and Z. Guo, *Polymer*, 2018, **138**, 203–210.

179 B. Luo, X. Wang, Y. Wang and L. Li, *J. Mater. Chem. A*, 2014, **2**, 510–519.

180 S. Liu and J. Zhai, *J. Mater. Chem. A*, 2015, **3**, 1511–1517.

181 B. Luo, X. Wang, Y. Wang and L. Li, *J. Mater. Chem. A*, 2013, **2**, 510–519.

182 S. K. Ghosh, A. Biswas, S. Sen, C. Das, K. Henkel, D. Schmeisser and D. Mandal, *Nano Energy*, 2016, **30**, 621–629.

183 A. Tamang, S. K. Ghosh, S. Garain, M. M. Alam, J. r. Haeberle, K. Henkel, D. Schmeisser and D. Mandal, *ACS Appl. Mater. Interfaces*, 2015, **7**, 16143–16147.

184 S. K. Ghosh, T. K. Sinha, B. Mahanty and D. Mandal, *Energy Technol.*, 2015, **3**, 1190–1197.

185 J. Fu, Y. Hou, M. Zheng, Q. Wei, M. Zhu and H. Yan, *ACS Appl. Mater. Interfaces*, 2015, **7**, 24480–24491.

186 A. A. Gandhi, M. Wojtas, S. B. Lang, A. L. Kholkin and S. A. Tofail, *J. Am. Ceram. Soc.*, 2014, **97**, 2867–2872.

187 M. Minary-Jolandan and M.-F. Yu, *Nanotechnology*, 2009, **20**, 085706.

188 M. M. Alam and D. Mandal, *ACS Appl. Mater. Interfaces*, 2016, **8**, 1555–1558.

189 S. K. Ghosh, P. Adhikary, S. Jana, A. Biswas, V. Sencadas, S. D. Gupta, B. Tudu and D. Mandal, *Nano Energy*, 2017, **36**, 166–175.

190 S. K. Ghosh and D. Mandal, *Appl. Phys. Lett.*, 2017, **110**, 123701.

191 S. K. Ghosh and D. Mandal, *ACS Sustainable Chem. Eng.*, 2017, **5**, 8836–8843.

192 K. Kim, M. Ha, B. Choi, S. H. Joo, H. S. Kang, J. H. Park, B. Gu, C. Park, C. Park, J. Kim, S. K. Kwak, H. Ko, J. Jin and S. J. Kang, *Nano Energy*, 2018, **48**, 275–283.

193 J.-S. Moon, W.-G. Kim, C. Kim, G.-T. Park, J. Heo, S. Y. Yoo and J.-W. Oh, *Mini-Rev. Org. Chem.*, 2015, **12**, 271–281.

194 B. Y. Lee, J. Zhang, C. Zueger, W.-J. Chung, S. Y. Yoo, E. Wang, J. Meyer, R. Ramesh and S.-W. Lee, *Nat. Nanotechnol.*, 2012, **7**, 351–356.

195 D.-M. Shin, H. J. Han, W.-G. Kim, E. Kim, C. Kim, S. W. Hong, H. K. Kim, J.-W. Oh and Y.-H. Hwang, *Energy Environ. Sci.*, 2015, **8**, 3198–3203.

196 C. M. Kelly, T. Northey, K. Ryan, B. R. Brooks, A. L. Kholkin, B. J. Rodriguez and N.-V. Buchete, *Biophys. Chem.*, 2015, **196**, 16–24.

197 A. Kholkin, N. Amdursky, I. Bdikin, E. Gazit and G. Rosenman, *ACS Nano*, 2010, **4**, 610–614.

198 V. Nguyen, R. Zhu, K. Jenkins and R. Yang, *Nat. Commun.*, 2016, **7**, 13566–13571.

199 L. Eppelbaum, *Geosciences*, 2017, **7**, 1–12.

200 Y. Lu, H. Tang, S. Fung, Q. Wang, J. Tsai, M. Daneman, B. Boser and D. Horsley, *Appl. Phys. Lett.*, 2015, **106**, 263503.

201 W. Wang and P. J. Thomas, *Sens. Actuators, A*, 2017, **263**, 113–121.

202 G. Nelson, R. Rajamani and A. Erdman, *Appl. Acous.*, 2014, **80**, 68–78.

203 C. Xiong, W. H. Pernice, J. H. Ngai, J. W. Reiner, D. Kumah, F. J. Walker, C. H. Ahn and H. X. Tang, *Nano Lett.*, 2014, **14**, 1419–1425.

204 M. Bauer, P. P. Franzreb, N. Spethmann and A. Widera, *Rev. Sci. Instrum.*, 2014, **85**, 96–101.

205 E. B. Magnusson, B. H. Williams, R. Manenti, M.-S. Nam, A. Nersisyan, M. J. Peterer, A. Ardavan and P. J. Leek, *Appl. Phys. Lett.*, 2015, **106**, 1509–1519.

206 Q. Zhao, M. Cao, J. Yuan, R. Lu, G. He and D. Wang, *Microsyst. Technol.*, 2014, **20**, 1317–1322.

207 G. T. Hwang, H. Park, J. H. Lee, S. Oh, K. I. Park, M. Byun, H. Park, G. Ahn, C. K. Jeong and K. No, *Adv. Mater.*, 2014, **26**, 4880–4887.

208 S. Lim, D. Son, J. Kim, Y. B. Lee, J. K. Song, S. Choi, D. J. Lee, J. H. Kim, M. Lee and T. Hyeon, *Adv. Funct. Mater.*, 2015, **25**, 375–383.

209 W. Zang, Y. Nie, D. Zhu, P. Deng, L. Xing and X. Xue, *J. Phys. Chem. C*, 2014, **118**, 9209–9216.

210 X. Xue, S. Wang, W. Guo, Y. Zhang and Z. L. Wang, *Nano Lett.*, 2012, **12**, 5048–5054.

211 Y. Hu and Z. L. Wang, *Nano Energy*, 2015, **14**, 3–14.

212 X. Xue, Y. Nie, B. He, L. Xing, Y. Zhang and Z. L. Wang, *Nanotechnology*, 2013, **24**, 225501.

213 W. Zang, P. Li, Y. Fu, L. Xing and X. Xue, *RSC Adv.*, 2015, **5**, 84343–84349.

214 Y. Li, Z. Zhang, G. Zhang, L. Zhao, S. Deng, N. Xu and J. Chen, *ACS Appl. Mater. Interfaces*, 2017, **9**, 3911–3921.

215 C. Liu, A. Yu, M. Peng, M. Song, W. Liu, Y. Zhang and J. Zhai, *J. Phys. Chem. C*, 2016, **120**, 6971–6977.

216 B. Yin, Y. Qiu, H. Zhang, J. Lei, Y. Chang, J. Ji, Y. Luo, Y. Zhao and L. Hu, *Nano Energy*, 2015, **14**, 95–101.

217 S. Lu, Q. Liao, J. Qi, S. Liu, Y. Liu, Q. Liang, G. Zhang and Y. Zhang, *Nano Res.*, 2016, **9**, 372–379.

218 M. Choi, G. Murillo, S. Hwang, J. W. Kim, J. H. Jung, C.-Y. Chen and M. Lee, *Nano Energy*, 2017, **33**, 462–468.

219 H. Liow Chi, X. Lu, F. Tan Chuan, H. Chan Kwok, K. Zeng, S. Li and W. Ho Ghim, *Small*, 2017, **14**, 1702268.

220 Y. Yu, H. Sun, H. Orbay, C. Feng, C. G. England, W. Cai and X. Wang, *Nano Energy*, 2016, **27**, 275–281.

221 S. K. Karan, R. Bera, S. Paria, A. K. Das, S. Maiti, A. Maitra and B. B. Khatua, *Adv. Energy Mater.*, 2016, **6**, 1601016.

222 J.-H. Lee, K. Y. Lee, M. K. Gupta, T. Y. Kim, D.-Y. Lee, J. Oh, C. Ryu, W. J. Yoo, C.-Y. Kang, S.-J. Yoon, J.-B. Yoo and S.-W. Kim, *Adv. Mater.*, 2014, **26**, 765–769.

223 S. Siddiqui, H. B. Lee, D. I. Kim, L. T. Duy, A. Hanif and N. E. Lee, *Adv. Energy Mater.*, 2018, **8**, 1701520.

224 X. Chen, H. Tian, X. Li, J. Shao, Y. Ding, N. An and Y. Zhou, *Nanoscale*, 2015, **7**, 11536–11544.

225 X. Chen, X. Li, J. Shao, N. An, H. Tian, C. Wang, T. Han, L. Wang and B. Lu, *Small*, 2017, **13**, 1604245.

226 A. Maitra, S. K. Karan, S. Paria, A. K. Das, R. Bera, L. Halder, S. K. Si, A. Bera and B. B. Khatua, *Nano Energy*, 2017, **40**, 633–645.

227 V. Vivekananthan, N. R. Alluri, Y. Purusothaman, A. Chandrasekhar, S. Selvarajan and S.-J. Kim, *ACS Appl. Mater. Interfaces*, 2018, **10**, 18650–18656.

228 S. K. Ghosh and D. Mandal, *Appl. Phys. Lett.*, 2016, **109**, 103701.

229 S. K. Ghosh and D. Mandal, *Nano Energy*, 2016, **28**, 356–365.

230 N. A. Hoque, P. Thakur, P. Biswas, M. M. Saikh, S. Roy, B. Bagchi, S. Das and P. P. Ray, *J. Mater. Chem. A*, 2018, **6**, 13848–13858.

231 S. Roundy, P. K. Wright and J. Rabaey, *Comput. Commun.*, 2003, **26**, 1131–1144.

232 J. J. Dosch, D. J. Inman and E. Garcia, *J. Intell. Mater. Syst. Struct.*, 1992, **3**, 166–185.

233 S. Song, Y. Hou, M. Guo, L. Wang, X. Tong and J. Wu, *Constr. Build. Mater.*, 2017, **131**, 57–65.

234 J. Zhang, Y. Lu, Z. Lu, C. Liu, G. Sun and Z. Li, *Smart Mater. Struct.*, 2015, **24**, 025023.

235 T. Q. Trung and N. E. Lee, *Adv. Mater.*, 2016, **28**, 4338–4372.

236 C. Lang, J. Fang, H. Shao, X. Ding and T. Lin, *Nat. Commun.*, 2016, **7**, 11108–11114.

237 Q. Feng, Q. Kong, L. Huo and G. Song, *Smart Mater. Struct.*, 2015, **24**, 115020.

238 P. Yu, W. Liu, C. Gu, X. Cheng and X. Fu, *Sensors*, 2016, **16**, 819–833.

239 M.-S. Kim, H.-R. Ahn, S. Lee, C. Kim and Y.-J. Kim, *Sens. Actuators, A*, 2014, **212**, 151–158.

240 X. Chen, J. Shao, N. An, X. Li, H. Tian, C. Xu and Y. Ding, *J. Mater. Chem. C*, 2015, **3**, 11806–11814.

241 L. Persano, C. Dagdeviren, Y. Su, Y. Zhang, S. Girardo, D. Pisignano, Y. Huang and J. A. Rogers, *Nat. Commun.*, 2013, **4**, 1633–1642.

242 Y. Jeong, M. Sim, J. H. Shin, J.-W. Choi, S. N. Cha, H. Choi, C. Moon and J. E. Jang, *RSC Adv.*, 2015, **5**, 40363–40368.

243 R. Krimholtz, D. A. Leedom and G. L. Matthaei, *Electron. Lett.*, 1970, **6**, 398–399.

244 V. Giurgiutiu, *J. Intell. Mater. Syst. Struct.*, 2005, **16**, 291–305.

245 J. Wang, Z. Shi, H. Xiang and G. Song, *Smart Mater. Struct.*, 2015, **24**, 105017.

246 X. Xu, D. Cao, H. Yang and M. He, *Int. J. Pavement Res. Technol.*, 2017, **11**, 388–395.

247 J. Zhu, S. C. M. Ho, D. Patil, N. Wang, R. Hirsch and G. Song, *Smart Mater. Struct.*, 2017, **26**, 107002.

248 Y. C. Hu, T. H. Lee, P. Z. Chang and P. C. Su, *Thin Solid Films*, 2015, **584**, 112–115.

249 Z. Yang and J. Zu, *IEEE/ASME Trans. Mechatron.*, 2016, **21**, 1787–1791.

250 K. Hyeoung Woo, B. Amit, P. Shashank, U. Kenji, M. Douglas, E. N. Robert and F. H. Heath, *Jpn. J. Appl. Phys.*, 2004, **43**, 6178–6183.

251 H.-H. Huang and K.-S. Chen, *Sens. Actuators, A*, 2016, **238**, 317–328.

252 J. Zhao and Z. You, *Sensors*, 2014, **14**, 12497–12510.

253 A. Toprak and O. Tigli, *J. Microelectromech. Syst.*, 2015, **24**, 1989–1997.